



Aerosol_cci+
Climate Assessment Report

REF : aerosol CAR
ISSUE : 3.1
DATE : 19.07.2022
PAGE : I




ESA Climate Change Initiative
Aerosol_cci+

Climate Assessment Report
Deliverable number D5.1c

Version 3.1

Document reference: Aerosol_cci+_CAR_3.1.doc

	Aerosol_cci+ Climate Assessment Report	REF : aerosol CAR ISSUE : 3.1 DATE : 19.07.2022 PAGE : II
---	---	--

DOCUMENT STATUS SHEET

	FUNCTION	NAME	DATE	SIGNATURE
contributing authors	Editors	T. Popp	10.03.2020	
Core users	Contributors	A. Benedetti S. Quesada-Ruiz S. Kinne	16.07.2020 16.03.2021 29.03.2021 28.04.2022 06.07.2022	
reviewed by	Science leader	T. Popp	28.07. 2020 31.03.2021 06.05.2022 19.07.2022	
approved by	Technical officer (ESA)	M. Eisinger		
issued by	Project manager	T. Popp		

	Aerosol_cci+ Climate Assessment Report	REF : aerosol CAR ISSUE : 3.1 DATE : 19.07.2022 PAGE : III
---	---	---

EXECUTIVE SUMMARY

The Climate Assessment Report evaluates test datasets processed with algorithms further developed under Aerosol_cci+ by conducting specific use cases and general simple overview analysis. It aims to identify strengths and weaknesses of the algorithms / datasets and to prove their added value for climate science and applications.

The report contains a light / visual user evaluation of several versions of the test datasets, and a description of two user case studies (setup and summaries of their results).

The two user case studies represent the two major application domains of Aerosol_cci datasets:

- Radiative forcing study, as example for climate research
- Data assimilation study, as example for reanalysis / long-term data records

Both user case studies apply test datasets processed in Aerosol_cci+ until early 2022 (final climate research data package) and – as far as available and needed – could also include longer time series processed with the same algorithm version (Swansea algorithm) under the C3S_312b_Lot2 contract of the Copernicus Climate Change Service where a major reprocessing was done in late 2020.

After definitions (sec. 1) and an introduction (sec. 2), this report summarizes the two user case studies on radiative forcing (sec. 3) and data assimilation (sec. 4) before concluding with a summary (sec. 5) and references (sec. 6)

	Aerosol_cci+ Climate Assessment Report	REF : aerosol CAR ISSUE : 3.1 DATE : 19.07.2022 PAGE : IV
---	---	--

Document change record

Issue	Date	Modified Items / Reason for Change
0.9	10. 03. 2020	First issue of the document
1.0	16. 07. 2020	Contributions by core users
1.1	28. 07. 2020	Review by science lead, final layout and editing
2.0	31. 03. 2021	Summaries of the two user case studies added Review and final integration by science leader
3.0	06.05.2022	Additional overview analysis added (pages 9-12, 28-34); updated executive summary, introduction and summary
3.1	19.07.2022	Revision based on ESA review: Updates of executive summary, introduction, section 4 (data assimilation user case study, conclusions).

LIST OF TABLES

Table 2.1 Overview of planned user-case studies 4
Table 4.1 Overview of assimilation experiments..... 35




LIST OF FIGURES

Figure 3.1	Seasonal global distributions of AOD properties from the 4 sensors.....	5
Figure 3.2	Seasonal global distributions of AOD differences to SLSTR/S3B	6
Figure 3.3	Annual global distributions of AOD properties compared to MODIS	7
Figure 3.4	Annual global distributions of AOD properties compared to MACv3	7
Figure 3.5	Seasonal global distributions of AOD differences compared to MACv3.....	8
Figure 3.6	2019 / 2020 combined AOD, AODf and AAOD of two SLSTR sensors.....	9
Figure 3.7	Differences of properties in Fig. 3.6 to the MAC aerosol climatology.....	10
Figure 3.8	Differences of properties in Fig. 3.6 to MISR data	11
Figure 3.9	Differences of properties in Fig. 3.6 to MISR data MODIS data	12
Figure 3.10	Annual global distributions for aerosol direct radiative effects at TOA.....	14
Figure 3.11	Annual global distributions for aerosol direct radiative effects at the surface	15
Figure 3.12	Annual global distributions for aerosol direct radiative effects in the atmosphere..	15
Figure 3.13	Annual global anthropogenic aerosol direct forcing at TOA.....	16
Figure 3.14	Annual global anthropogenic aerosol direct radiative effects at the surface.....	17
Figure 3.15	Annual global anthropogenic aerosol direct radiative effects in the atmosphere....	18
Figure 3.16	Annual global total anthropogenic aerosol radiative forcing at TOA.....	18
Figure 3.17	Annual global total anthropogenic aerosol radiative effects at the surface.....	19
Figure 4.1	AOD comparisons January 2019: CAMS, SLSTR SU 3A and 3B	22
Figure 4.2	AOD comparisons February 2019: CAMS, SLSTR SU 3A and 3B.....	22
Figure 4.3	AOD comparisons March 2019: CAMS, SLSTR SU 3A and 3B	23
Figure 4.4	AOD comparisons April 2019: CAMS, SLSTR SU 3A and 3B	23
Figure 4.5	AOD comparisons May 2019: CAMS, SLSTR SU 3A and 3B	24
Figure 4.6	AOD comparisons June 2019: CAMS, SLSTR SU 3A and 3B	24
Figure 4.7	AOD comparisons July 2019: CAMS, SLSTR SU 3A and 3B.....	25
Figure 4.8	AOD comparisons August 2019: CAMS, SLSTR SU 3A and 3B.....	25
Figure 4.9	AOD comparisons September 2019: CAMS, SLSTR SU 3A and 3B	26
Figure 4.10	AOD comparisons October 2019: CAMS, SLSTR SU 3A and 3B	26
Figure 4.11	AOD comparisons November 2019: CAMS, SLSTR SU 3A and 3B	27
Figure 4.12	AOD comparisons December 2019: CAMS, SLSTR SU 3A and 3B	27
Figure 4.13	AOD comparisons January 2020: CAMS, SLSTR CISAR, SU 3A, 3B.....	30
Figure 4.14	AOD comparisons February 2020: CAMS, SLSTR CISAR, SU 3A, 3B.....	30
Figure 4.15	AOD comparisons March 2020: CAMS, SLSTR CISAR, SU 3A, 3B.....	31
Figure 4.16	AOD comparisons April 2020: CAMS, SLSTR CISAR, SU 3A, 3B.....	31
Figure 4.17	AOD comparisons May 2020: CAMS, SLSTR CISAR, SU 3A, 3B.....	32
Figure 4.18	AOD comparisons June 2020: CAMS, SLSTR CISAR, SU 3A, 3B.....	32
Figure 4.19	AOD comparisons July 2020: CAMS, SLSTR CISAR, SU 3A, 3B.....	33
Figure 4.20	AOD comparisons August 2020: CAMS, SLSTR CISAR, SU 3A, 3B.....	33
Figure 4.21	AOD comparisons September 2020: CAMS, SLSTR CISAR, SU 3A, 3B.....	34
Figure 4.22	AOD comparisons October 2020: CAMS, SLSTR CISAR, SU 3A, 3B.....	34
Figure 4.23	AOD comparisons November 2020: CAMS, SLSTR CISAR, SU 3A, 3B.....	35
Figure 4.24	AOD comparisons December 2020: CAMS, SLSTR CISAR, SU 3A, 3B.....	35
Figure 4.25	Time series of AERONET AOD FC-Obs bias for the main experiments	38
Figure 4.26	Same as figure 4.13 but for Root Mean Square (RMS) error.	38
Figure 4.27	Same as figure 4.13 but for Modified Normalized Mean Bias (MNMB).	39
Figure 4.28	Same as figure 4.13 but for Fractional Gross Error (FGE).	39
Figure 4.29	Same as figure 4.13 but for Correlation coefficient.	40
Figure 4.30	Same as figure 4.13 but for as a function of forecast range.	40
Figure 4.31	Same as figure 4.18 but for RMS error.	41
Figure 4.32	Same as figure 4.18 but for MNMB error.	41
Figure 4.33	Same as figure 4.18 but for FG error.	42
Figure AA.1	Example of Voronoi polygons.	50
Figure AA.2	AERONET station map.	50



TABLE OF CONTENTS

DOCUMENT STATUS SHEET	II
EXECUTIVE SUMMARY	III
LIST OF TABLES	V
LIST OF FIGURES	VI
TABLE OF CONTENTS.....	VII
1 DEFINITIONS AND ABBREVIATIONS	1
2 INTRODUCTION.....	4
3 RADIATIVE FORCING	5
4 DATA ASSIMILATION.....	20
5 SUMMARY.....	53
6 REFERENCES	55

	Aerosol_cci+ Climate Assessment Report	REF : aerosol CAR ISSUE : 3.1 DATE : 19.07.2022 PAGE : 1
---	---	---

1 DEFINITIONS AND ABBREVIATIONS

This section summarizes the major definitions relevant for the validation report.

AAOD (Absorption Aerosol Optical Depth) is the vertically normalized atmospheric column integrated aerosol absorption at a certain wavelength (usually at 550 nm, the reference wavelength in global modelling) [note, $AAOD = AOD \cdot (1 - SSA)$]

AeroCom is an open science initiative founded to inter-compare aerosol modules in global modelling and evaluate overall model performance as well as the treatment of specific aerosol processes against available (and trusted) observations.

AERONET represents a federated network of globally distributed ground-based CIMEL sun-/sky-photometers, which is maintained (calibration facility, data processing and aerosol and water vapor products access) by NASA (National Aeronautics and Space Administration) and PHOTONS (PHOtométrie pour le Traitement Opérationnel de Normalisation Satellitaire)

AOD (Aerosol Optical Depth) is the vertically normalized atmospheric column integrated aerosol extinction at a certain wavelength or waveband (usually at 550nm, the reference wavelength in modelling). AOD is also often referred to as Aerosol Optical Thickness (AOT).

AODf (Fine-mode Aerosol Optical Depth) is the vertically normalized atmospheric column integrated aerosol extinction at a certain wavelength or waveband (usually at 550nm) of aerosol particles smaller than 0.5µm in radius (or smaller 1µm in diameter).

ATSR (Along Track Scanning Radiometer) was a multi-channel imaging radiometer (with dual view capabilities in the visible and near-IR solar spectrum). Two versions are used for aerosol retrieval: ATSR-2 on board of the European Space Agency's ERS-2 satellite (1995-2002) and the advanced ATSR (AATSR) on ESA's ENVISAT satellite (2002-2012).

CF (Climate and Forecast) naming convention metadata are designed to promote the processing and sharing of files created with the NetCDF API.

CMUG (Climate Model User Group) is a part of ESA's Climate Change Initiative (CCI) and is composed of members of major climate research institutes in Europe. The group is tasked to oversee the usefulness of new climate data records produced for CCI selected ECVs.

ECV (Essential Climate Variables) are geo-physical quantities of the Earth-Atmosphere-System that are technically and economically feasible for systematic (climate) observations.

	Aerosol_cci+ Climate Assessment Report	REF : aerosol CAR ISSUE : 3.1 DATE : 19.07.2022 PAGE : 2
---	---	---

ENVISAT ("Environmental Satellite") is a now inoperative ESA polar-orbiting (ca 10am local overpass) satellite, which supplied between 2002 and 2012 atmospheric data, including for aerosol remote sensing relevant AATSR, MERIS and GOMOS sensor data.

ESA (European Space Agency) is the European Organisation for Space Research with Headquarters in Paris.

FCDR (Fundamental Climate Data Records or simply **CDR**) represent long-term records of measurements or retrieved physical quantities from remote sensing. FCDRs require consistency across multiple platforms with respect to (1) calibration, (2) algorithms, (3) spatial and temporal resolution, (4) quantification of errors and biases and (5) data format. FCDRs also need to manifest applied ancillary data.

FMF (Fine Mode Fraction) is the fraction of the total AOD which is contributed by aerosol particles smaller than 1µm in diameter. Due to their smaller size these aerosol particles are referred to as fine-mode aerosol, in contrast to (larger or) coarse mode aerosol particles.


GCOS (Global Climate Observing System), located at WMO in Geneva, is intended to be a long-term, user-driven operational system capable of providing the comprehensive observations required for (1) monitoring the climate system, (2) detecting and attributing climate change, (3) assessing impacts of, and supporting adaptation to, climate variability and change, (4) application to national economic development and (5) research to improve understanding, modelling and prediction of the climate system.

GRASP (Generalized Retrieval of Aerosol and Surface Properties) is an aerosol retrieval algorithm that processes properties of aerosol- and land-surface-reflectance. It infers nearly 50 aerosol and surface parameters including particle size distribution, the spectral index of refraction, the degree of sphericity and absorption.

CAMS (Copernicus Atmosphere Monitoring Service), operational service in the **Copernicus** program which monitors and predicts global distributions and long-range transports of greenhouse gases (carbon dioxide, methane), of aerosols that result from both natural processes and human activities and of reactive gases (tropospheric ozone, nitrogen dioxide). CAMS also evaluates how these constituents influence climate and estimates their sources and sinks.

MISR (Multi-angle Imaging Spectro-Radiometer) is a multi-spectral sensor on NASA's EOS Terra platform with (9) multi-directional view capabilities.

MODIS (Moderate Resolution Imaging Spectro-Radiometer) is a multi-spectral sensor on NASA's EOS Terra and Aqua platforms.

	Aerosol_cci+ Climate Assessment Report	REF : aerosol CAR ISSUE : 3.1 DATE : 19.07.2022 PAGE : 3
---	---	---

NASA (National Aeronautics and Space Administration), the civil US federal authority for space and aircraft research founded in 1958 with headquarters in Washington, D.C.

POLDER (POLarization and Directionality of the Earth's Reflectances) was a passive optical imaging radiometer and polarimeter for studies on radiative and microphysical properties of clouds and aerosols on the French CNES PARASOL (Polarization and Anisotropy of Reflectances for Atmospheric Sciences coupled with Observations from a Lidar), in orbit until 2013.

SLTSR (Sea and Land Surface Temperature Radiometer) on-board SENTINEL-3 is to maintain continuity with the (A)ATSR series of instruments. Additional new features include a wider swath, new channels (including two channels dedicated to fire detection), and higher resolution in some channels.

SSA (Single Scattering Albedo) quantifies the likelihood of scattering during an attenuation (or 'extinction') event by an atmospheric particle of given size and shape at a certain wavelength (most important at 550 nm, the reference wavelength in global modeling). The remaining fraction, 1-SSA referred to co-single scattering albedo, quantifies the likelihood of absorption during an attenuation (or extinction) event.

2 INTRODUCTION

In 2010 ESA's Aerosol_cci set out to develop and improve aerosol retrievals for European satellite sensors. These new products permitted new science studies. In order to demonstrate useful applications selected 'user-case' studies were supported. The results of these user case studies were summarized in the Climate Assessment Report (CAR) at the end of the Aerosol_cci2 project (Aerosol_cci2 CAR, v2.7, 08.01.2018) which contained eight different user case studies for the variety of Aerosol_cci2 datasets (e.g. AOD records from ATSR-2 / AATSR dual view sensors, stratospheric extinction record from GOMOS star occultation, dust AOD from IASI thermal infrared spectrometers, absorbing aerosol index from UV-VIS spectrometers).

This extension of Aerosol_cci (under the name "Aerosol_cci+") focused on only the instruments of the dual view sensor line (ATSR-2, AATSR, SLSTR) to optimize a data record covering the periods 1995 – 2012 (ATSR-2, AATSR) and extending it with the period since 2016 (SLSTR onboard SENTINEL-3A and SENTINEL-3B). Intensive validation of Aerosol_cci2 datasets was conducted by comparison to external reference datasets (AERONET ground-based sun photometers, other established satellite aerosol datasets) and documented in the Product Validation and Inter-comparison Reports (PVIR v3.41, 21.12.2017 and PVIR v4.2, 09.01.2019 after a small extension through a bridging option) which identified algorithm weaknesses and needs for further algorithm improvements. The goal of the Aerosol_cci+ project (2019 – 2022) was to achieve some of those intended improvements and evaluate them again through validation against external reference data and through conducting two user case studies listed in Tab. 2.1.

Table 2.1 overview of planned user-case studies

user case study	chapter	institute	lead author
Aerosol radiative forcing	3	MPI-Met	Stefan Kinne
Assimilation of SLSTR into CAMS model	4	ECMWF	Angela Benedetti

For both user case studies the Climate Assessment report contains in the following two sections an assessment of different versions of the test datasets (from two algorithms, the mature Swansea algorithm applied to all 4 sensors, and the innovative CISAR / Rayference algorithm applied to SLSTR onboard Sentinel-3A) available under Aerosol_cci+ and a summary of each of the two user case studies.

Advanced test dataset versions have become available by end of 2020 as 2nd climate research data package and early 2022 as 3rd climate research data package. These include global aerosol retrievals processed with the latest versions of the Swansea algorithm for the year 1998 (ATSR2 sensor), 2008 (AATSR sensor) 2019 and 2020 (SLSTR sensors on Sentinel-3A and Sentinel-3B, processed under the operational C3S_312b_Lot2). In addition, also an innovative algorithm CISAR by Rayference has been applied to SLSTR September – December 2019 data (covering initially 2/3 of the globe) and with a 2nd version covering all of 2020.

3 RADIATIVE FORCING

Overview of the user case study

The user case study on radiative forcing associates aerosol satellite retrievals of ESA's aerosol CCI+ project with aerosol radiative effects. In off-line radiative transfer simulations aerosol impacts on three atmospheric radiative properties are examined:

- aerosol impacts on radiative net-fluxes at the **top of the atmosphere (TOA)**, which are relevant for climate (change) studies
- aerosol impacts on radiative net-fluxes at the **surface**, which control surface exchange processes
- aerosol impacts on radiative net-fluxes in the **atmosphere** (as differences of the previous two net-flux impacts), which represents the (solar) heating in atmospheric aerosol layers and hereby affects atmospheric dynamics.

The applied data

The applied satellite data are monthly gridded (1x1 deg) averages for aerosol column load (aerosol optical depth, AOD at 550nm) and aerosol column load associated with sub-micrometer sizes (fine mode AOD at 550nm). These AOD and AODf data are based on Uni. of Swansea retrievals for dual-view and multi-spectral ATSR heritage sensor data. In this study retrieval data from 3 different years were applied in time-steps of at least 10 years with the potential to examine also decadal change. 1998 are based on ATSR2 sensor data, 2008 data are based on AATSR sensor data and of 2020 data are on SLSTR sensor data on two different platforms (Sentinel-3 A and B). The seasonal AOD and AODf averages of these data are presented in Figure 3.1.

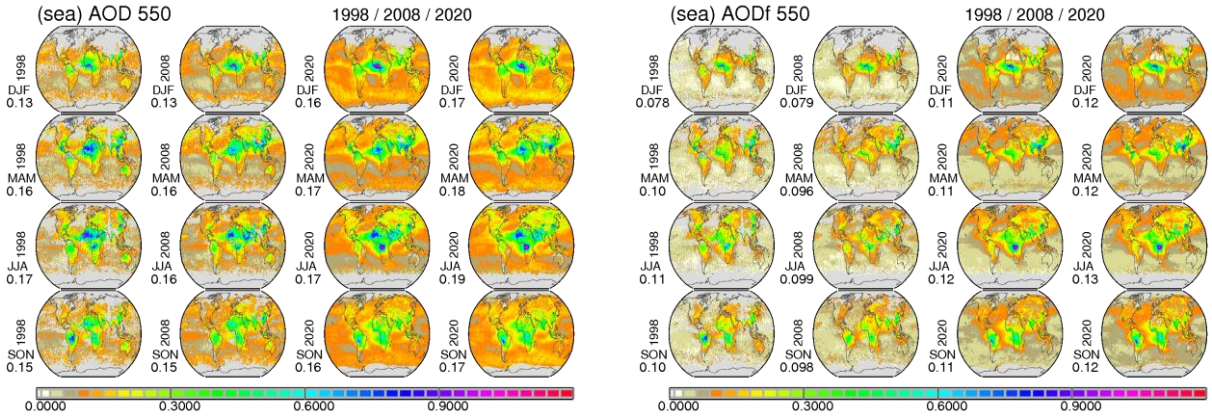


Figure 3.1 Seasonal global distributions of AOD,550nm (left block) and AODf,550nm (right block) retrievals by ATSR2 1998 data (col1), AATSR 2008 (col2), SLSTR Sentinel-3A 2020 (col3) and SLSTR Sentinel-3B 2020 (col4). Values to the lower left indicate seasonal annual averages.

The decadal changes

Seasonal differences between 1998, 2008 and 2020 AOD and AODf retrievals (as anomalies to the same SLSTR Sentinel-3 B 2020 reference) are presented in Figure 3.2.

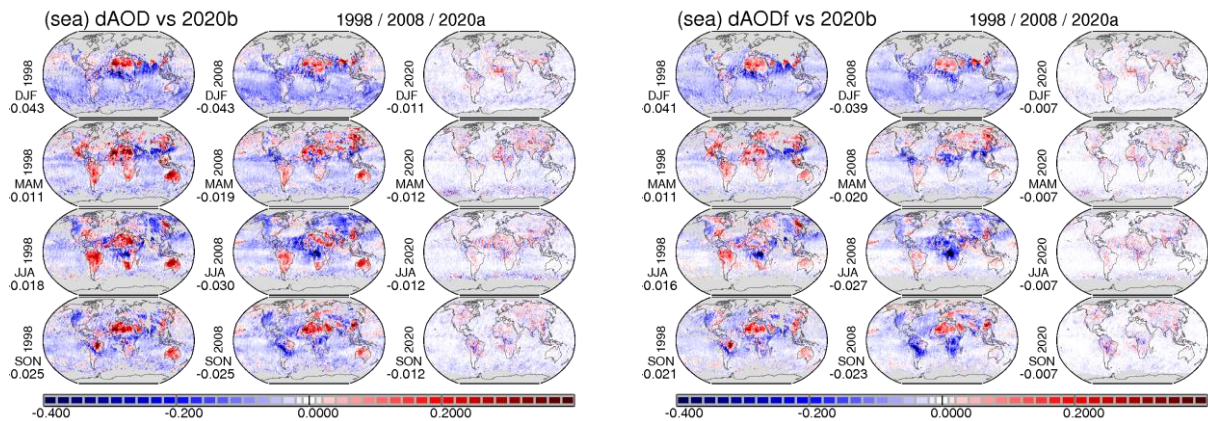


Figure 3.2: Seasonal global distributions differences for AOD,550nm (left block) and AODf,550nm (right block) between ATSR2 1998 (col1), AATSR 2008 (col2) and SLSTR Sentinel-3A 2020 (col3) data with respect to SLSTR Sentinel-3B 2020 data. Values to the lower left indicate global seasonal differences.

While seasonal differences between the two SLSTR 2020 data sets are relatively small (different sign meridional striping suggests retrieval limitations at wider swath angles) there are consistent regional differences to older AATSR and ATSR2: Aside from larger AOD values over oceans (and even for AODf during DJF) the largest differences are over continents. Most prominently are smaller SLSTR AOD over the Sahara (though mainly by AODc during dust seasons), over South America, East Asia and Australia (there mainly by AODc). In contrast, SLSTR AODf (and thus also AOD) during JJA over the Congo region are significantly larger. But there are also differences of earlier ATSR2 to AATSR retrievals with larger AODf (and AOD) during dust seasons over the Sahara and during the biomass season over South America. While expected long-term regional trends (i.e. linked to emission data) can be identified (e.g. reduced biomass burning over South America, increased pollution over India and decreased pollution over Europe) the anomalies seem overpaced by anomalies from retrieval differences and possibly also by biases for any of the three selected years. Thus, even though the SLSTR AOD and AODf are higher (mainly during DJF) it seems premature to combine these data for decadal trends.

Quick evaluations

The previous 'STR' retrieval comparisons did not answer if presented distributions are correct or biased. For a retrieval quality assessment, comparisons are presented to commonly used MODIS (-terra) retrievals for the same year in Figure 3.3 and in a more general sense to the MACv3 aerosol climatology in Figures 3.4 and 3.5 for AOD and

the contributing fine-mode and coarse-mode fractions. Note, that for MODIS no 1998 are available and no continental AODf for 2020 were processed.

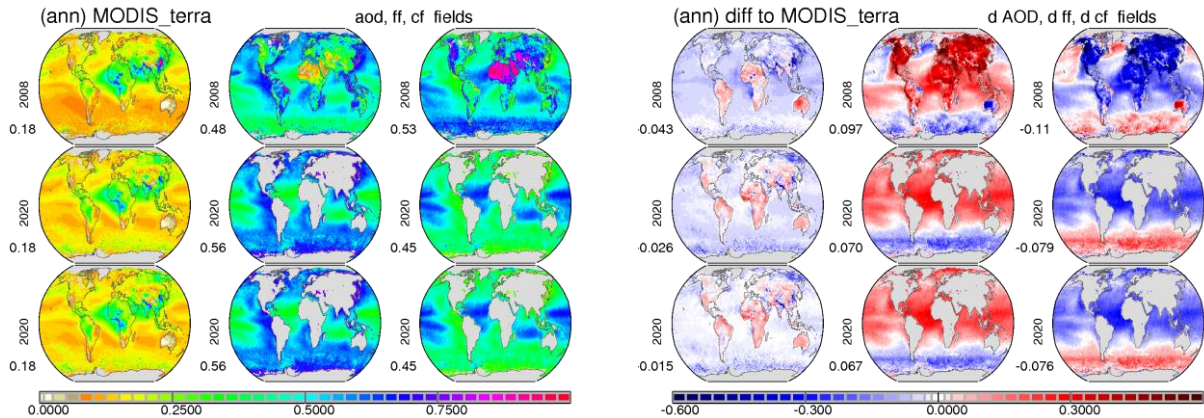


Figure 3.3: Annual global distributions of AOD,550nm (col1), fine-mode AOD fraction (col2) and coarse mode AOD fraction (col3) by MODIS-Terra retrievals for years 2008 (row1) and 2020 (row 2,3) are presented in the left block. Differences between AATSR or SLSTR data with respect to these MODIS data are presented in the right block. Values to the lower left indicate global annual averages (left block) and differences (right block). (Note that MODIS retrievals are not available for the year 1998 and 2020 AODf data were not yet processed over continents).

AATSR and SLSTR suggest smaller AOD over oceans, which, however, is more in line with MISR retrievals and global modeling. In contrast, AATSR and SLSTR have larger AOD data than MODIS over lower latitude continents and Australia. Overall global AOD averages of AATSR and SLSTR are lower by 0.04 and 0.02 than MODIS but the biggest difference are much higher AOD assignments to smaller aerosol sizes especially in dust dominated regions, where higher super-size aerosol contributions are expected. – also for S, (higher) and super-micrometer sizes.

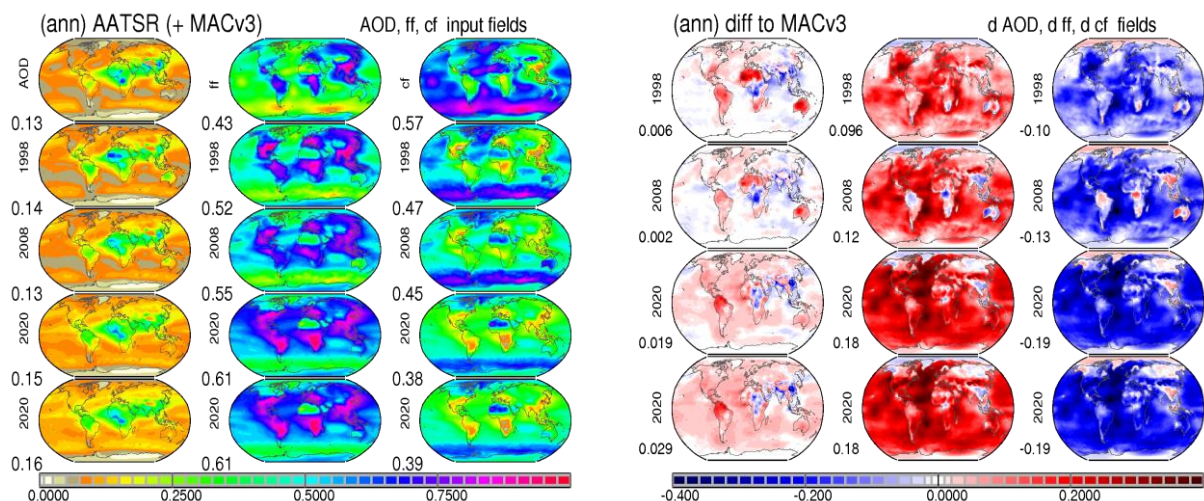


Figure 3.4: Annual global distributions of absolute values (left block) and differences to MACv3 (right block). AOD,550nm (col1), fine-mode AOD fraction (col2) and coarse-mode AOD fraction (col3) are presented for MACv3 (row1) and retrievals by ATSR2 in 1998 (row2), AATSR in 2008 (row3), SLSTR Sentinel-3A (row4) and SLSTR Sentinel-3B (row5) in 2020. Values to the lower left indicate global annual averages (left) or differences (right). Only larger deviations to the general MACv3 data are meaningful.

Also, the comparisons to MACv3 confirm the unexpected high AOD attribution to the fine mode which are particularly large over oceans – especially for SLSTR data. For more detail AOD, AODf and AODc seasonal differences to MACv3 are now analyzed (note, without the MACv3 link a particular year only larger deviations are meaningful).

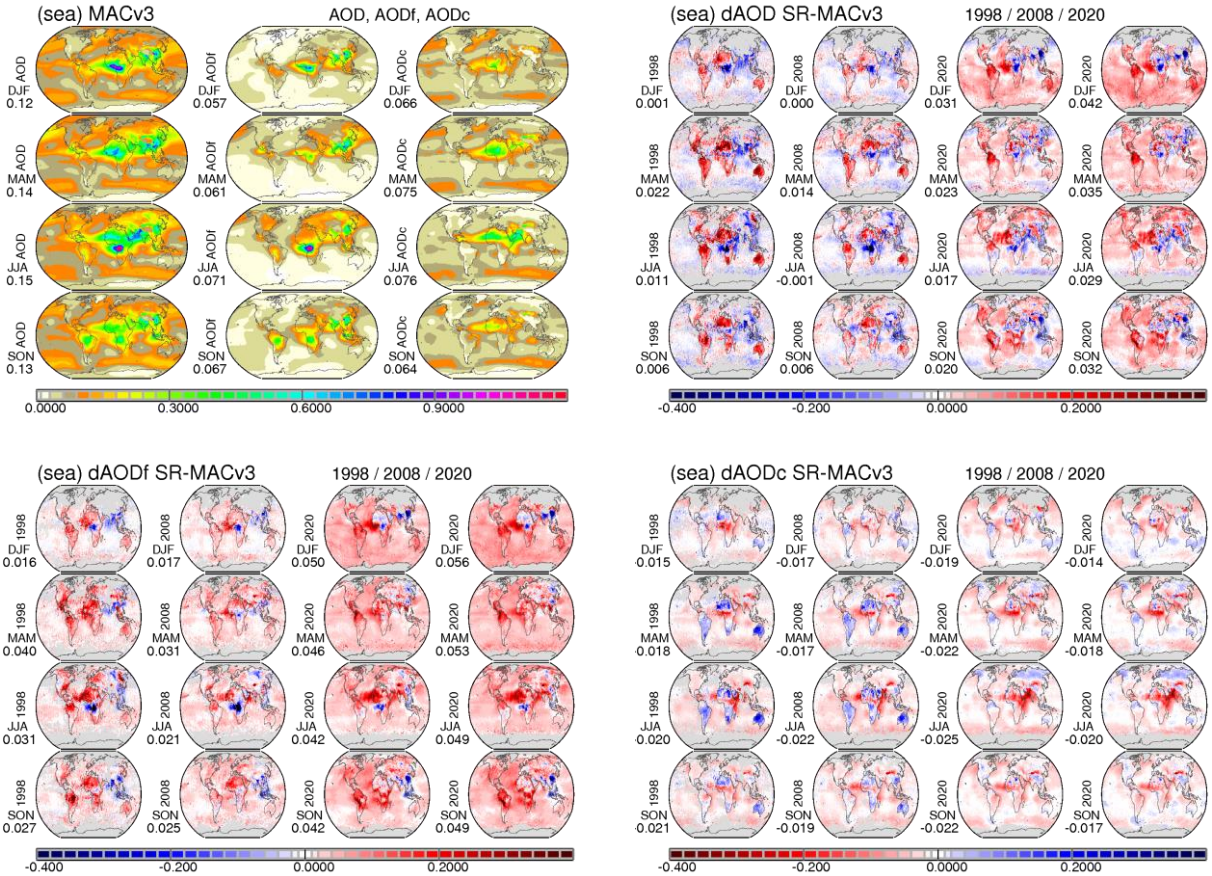


Figure 3.5: Seasonal global distributions of AOD,550nm (col1), fine-mode AOD (col2) and coarse mode AOD (col3) by the MACv3 aerosol climatology (top left) and for AOD (top right), AODf (bottom left) and AODc (bottom right) seasonal distribution differences of 'STR' satellite retrievals with respect to MACv3 climatology for ATSR2 retrievals of 1998 (col1), for AATSR retrievals of 2008 (col2) and for SLSTR Sentinel-3A and Sentinel-3B retrievals of 2020 (col3,4). Values to the lower left indicate global seasonal MACv3 averages or differences to MACv3.

On average AODf values (in comparisons to suggestions by MACv3) are globally larger by 0.035, 0.025 and even 0.050 for ATSR2, AATSR and SLSTR, respectively. AODf retrievals are higher for dust dominated regions. In addition, for ATSR2 AODf retrievals are larger over continents and for SLSTR AODf retrievals are much higher over oceans. On average AODc values (in comparison to suggestions by MACv3) are globally slightly smaller by 0.02. AODc is underestimated over continental high latitudes for (backward viewing) ATSR2 and AATSR in the SH whereas for (forward viewing) SLSTR in the NH.



Further overview evaluation combined for 2019 / 2020 and both SLSTR instruments

For a general evaluation of SLSTR retrievals the combined retrievals of mid-visible AOD and AODf – along with their derived AODc and FMF properties – were analyzed spatially and seasonally on a global scale in comparisons to (1) the MAC-climatology, to same period MISR retrievals and to same period MODIS retrievals. The selected 2-year period covers the years of 2019 and 2020. And for SLSTR statistics, data from operating sensors on two different platforms are combined. Seasonal maps for AOD, AODf, AODc and FMF are presented in Figure 3.6 and difference maps to data from MAC, MISR retrievals and MODIS retrievals are presented in Figures 3.7, 3.8 and 3.9. Larger SLSTR biases are relatively high fine-mode contributions to compensate for missed coarse-mode contributions. This is also reflected in relatively larger FMF.

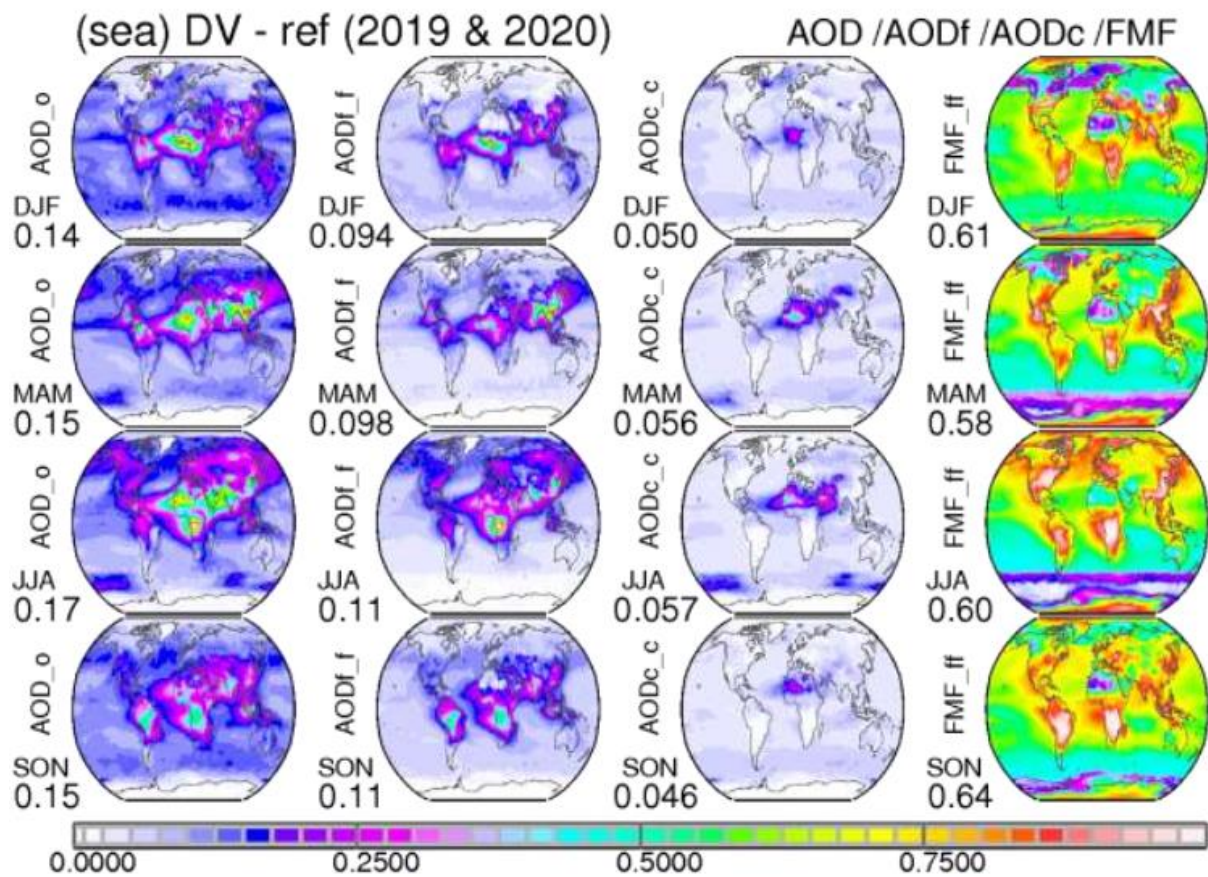


Figure 3.6: Based on 2019 and 2020 AOD, AODf and AAOD retrievals of two SLSTR sensors the combined seasonal properties for AODf, AODc (=AOD-AODf), FMF (=AODf/AOD) and SSA (=1-AAOD/AOD) are presented. Values indicate global seasonal averages.

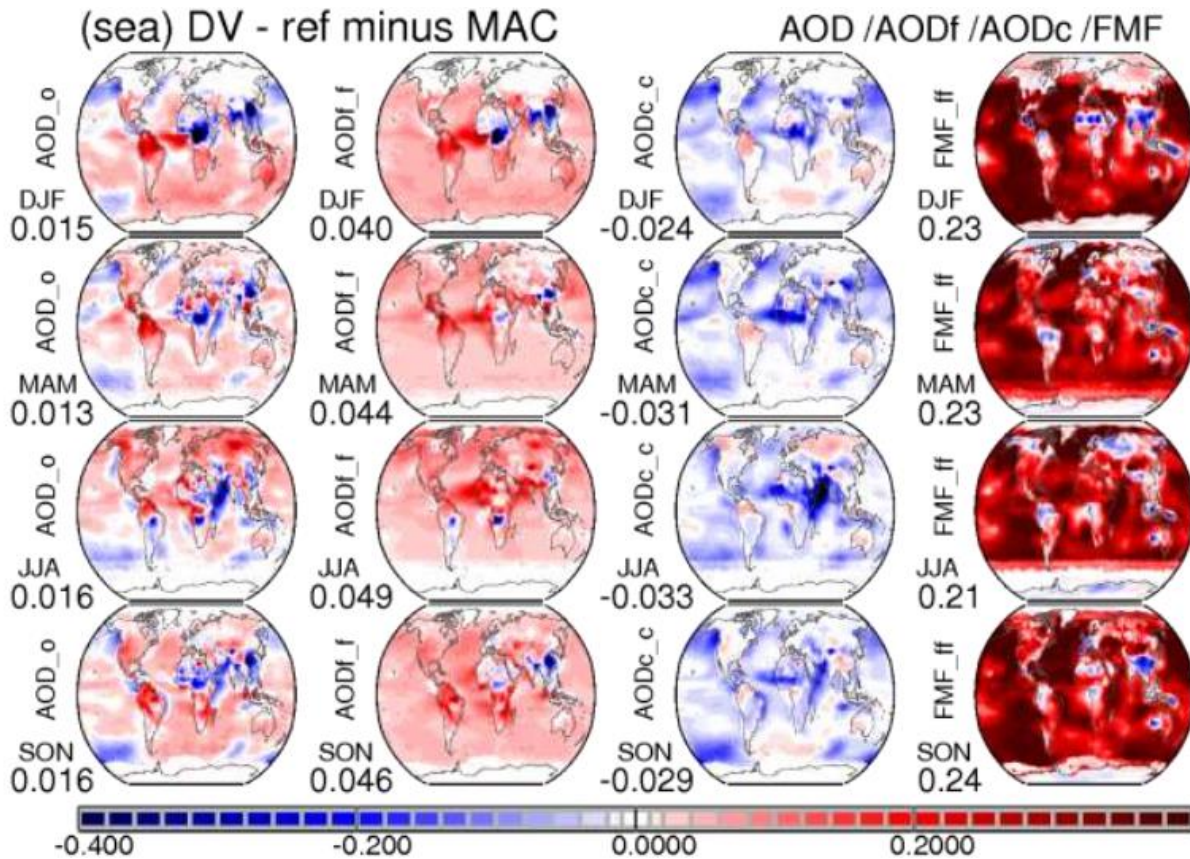


Figure 3.7: Differences to the properties of Figure 1 to those of the (year independent) MAC aerosol climatology. Values indicate global seasonal differences.

The major SLSTR biases *if the MAC climatology is the considered as reference* are:

- pattern of over- and under-estimates in total AOD driven by fine-mode and coarse mode biases
- fine-mode AOD overestimates for dust outflow over oceans, over biomass regions and over oceans
- coarse-mode AOD underestimates for dust outflow, over central Africa, Arabia and over oceans
- much higher fine-mode AOD fractions over oceans

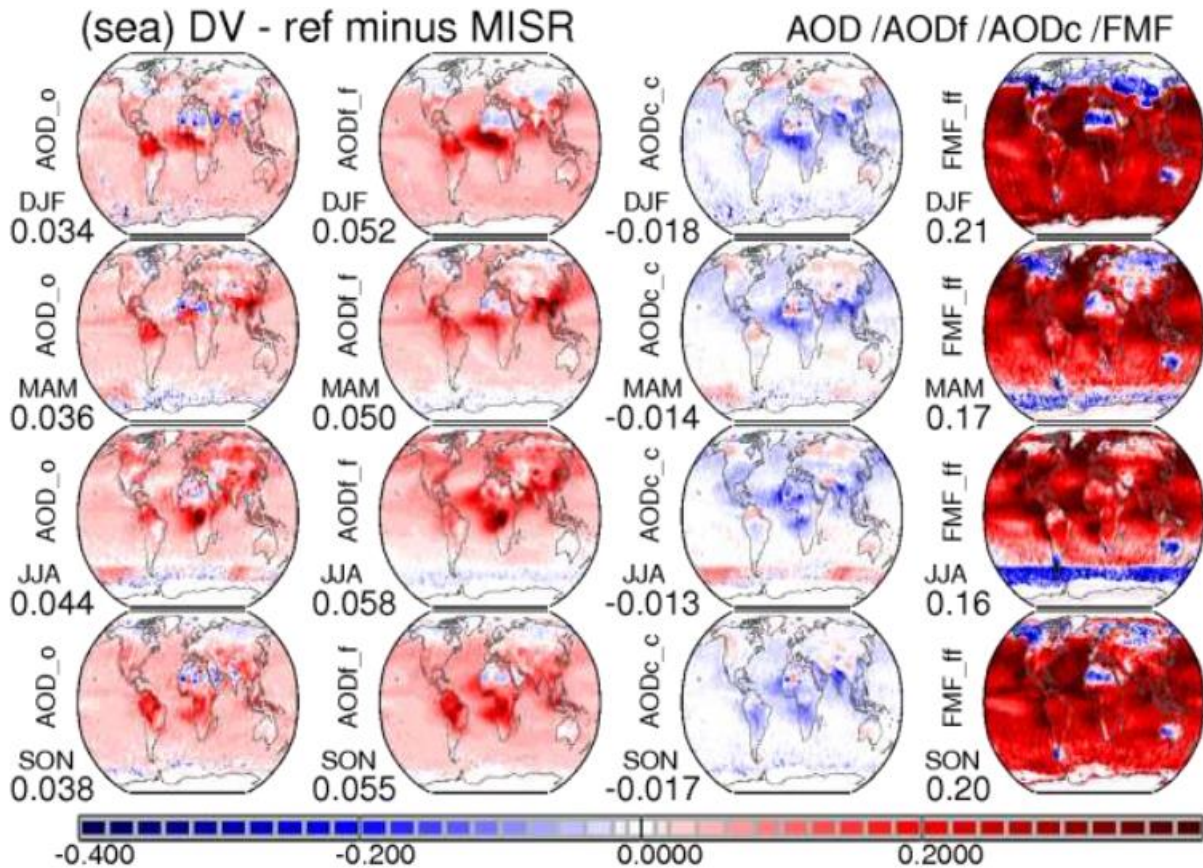


Figure 3.8: Differences to the properties of Figure 1 to those of the MISR data for the same 2019/2020 period. Note that the MISR fine-mode definition has a much smaller size threshold. Values indicate global seasonal differences.

The major SLSTR biases if MISR is the considered as reference (due to the much lower fine-mode/coarse mode separation size, only total AOD differences are commented) are:

- ocean AOD background is higher (MISR has the lowest oceanic background values among all satellite retrievals)
- continental AOD values are generally too high especially near wildfire
- underestimates for Saharan mineral dust and North Indian pollution

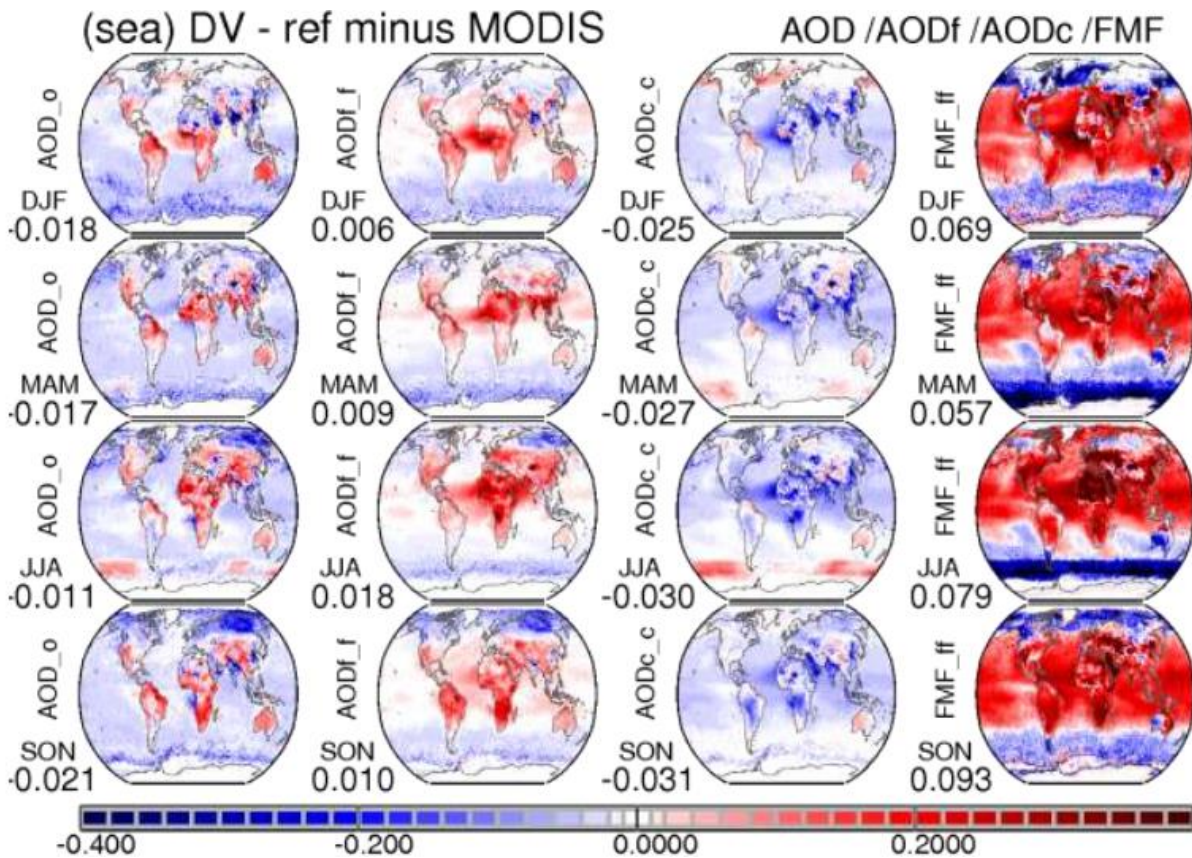


Figure 3.9: Differences to the properties of Figure 1 to those of the MODIS data for the same 2019/2020 period. Values indicate global seasonal differences.

The major SLSTR biases if MODIS is the considered as reference are:

- ocean AOD background is lower (but here MODIS is likely too high due to cloud contamination, which is also consistent that these are coarse-mode differences)
- continental AOD from tropics to mid-latitudes is generally too high, with very large fine-mode over-estimates, which are compensated by coarse-mode under-estimates - the SLSTR tendency to attribute AOD more to the fine-mode than the coarse-mode is obvious for dust outflow region where total AOD biases are small
- continental high-latitude AOD/AODf underestimates of boreal and wildfire events
- much higher fine-mode AOD fractions – except for the higher latitude winter periods over oceans

	Aerosol_cci+ Climate Assessment Report	REF : aerosol CAR ISSUE : 3.1 DATE : 19.07.2022 PAGE : 13
---	---	--

Radiative transfer simulations

Simulations of atmospheric radiative transfer apply a two-stream radiative transfer scheme. The spectral variability of atmospheric particle properties is represented by separate simulations in eight solar and twelve infrared sub-spectral bands. And in those bands a total of 120 exponential terms are used to represent the atmospheric trace-gas absorption. The vertical distribution of atmospheric properties is approximated by twenty plane-parallel homogenous layers and atmospheric state and trace-gas properties in these layers are defined by AFGL standard atmospheres. Land surface (VIS and n-IR) albedo data of MODIS are prescribed and the snow and ice coverage is based on NOAA microwave data. Cloud cover and cloud optical depth are represented by multi-annual monthly ISCCP data and eight simulations with applicable weights for all possible permutations (for high-, mid- and low- altitude cloud cover combinations). Simulations at each (of the 64800 1x1deg lat/lon) grid locations are done with monthly averages. For monthly solar radiative effects simulations at nine different solar zenith angles are weighted by their daytime fractions.

For aerosol, AOD and AODf of ATSR2, AATSR and SLSTR are prescribed to replace those of the MACv3 aerosol climatology. In that climatology a monthly ICAP background for AODc and AODf (based on 6 hourly 2015 to 2019 data) and a monthly AeroCom modeling background for aerosol absorption are modified according to differences to monthly AERONET and MAN statistics. Global modeling also provides information on aerosol vertical distribution and on today's anthropogenic AODf fraction. For the aerosol indirect effect by anthropogenic aerosol a simple CDNC to AODf relationship from satellite retrievals over ocean are applied. This relationship translates AODf increases at a given AODf (e.g. pre-industrial) background into a CDNC increase. Associated cloud droplet decreases (assuming no changes to the cloud water content) are then applied to the low altitude clouds.

Radiative impacts in the atmosphere are defined by differences of two simulations between a modified and a standard configuration. All simulations consider ISCCP tropospheric clouds. These 'dual-call' radiative transfer applications investigate

- ***all aerosol presence impact*** (*total direct radiative effect*)
- ***extra anthropogenic aerosol presence impact*** (*anthropogenic direct effect*)
- ***extra anthropogenic aerosol presence and reduced droplet radii impact*** (*anthropogenic direct and indirect radiative effects*)

Dual-call radiative transfer cannot consider climate feedbacks. Long-term Earth System Model (ESM) simulations with a fixed sea-surface temperature, however, suggests that atmospheric feedbacks are at most 10%. Thus, by ignoring radiative forcing feedbacks, no major extra errors are expected. It also should be pointed out that a dual-call scheme offers more precise answers, as internal (cloud) variability of independent ESM simulations is avoided.

Aerosol radiative effects (in Figures 3.6 to 3.9 for today's total aerosol and in Figures 3.10 to 3.13 for today's anthropogenic aerosol) are determined with each of the four AOD/AODf data-sets: 1998 ATSR2, 2008 AATSR and 2020 SLSTR Sentinel-3 A and B.

Total aerosol radiative effects – at TOA

The all aerosol direct TOA radiative effect varies globally between - 0.8 and -1.2 W/m², with the stronger cooling associated with the most recent SLSTR data. On a regional basis the TOA aerosol radiative effects vary between -10 and +25 W/m², with the strongest cooling in dust outflow over oceans and the strongest warming over desert region. The solar effect is a cooling, except over bright deserts and bright snow/ice of polar regions. For elevated (even weakly) absorbing dust the associated greenhouse effect causes a significant warming, which is largely responsible for the peak warming.

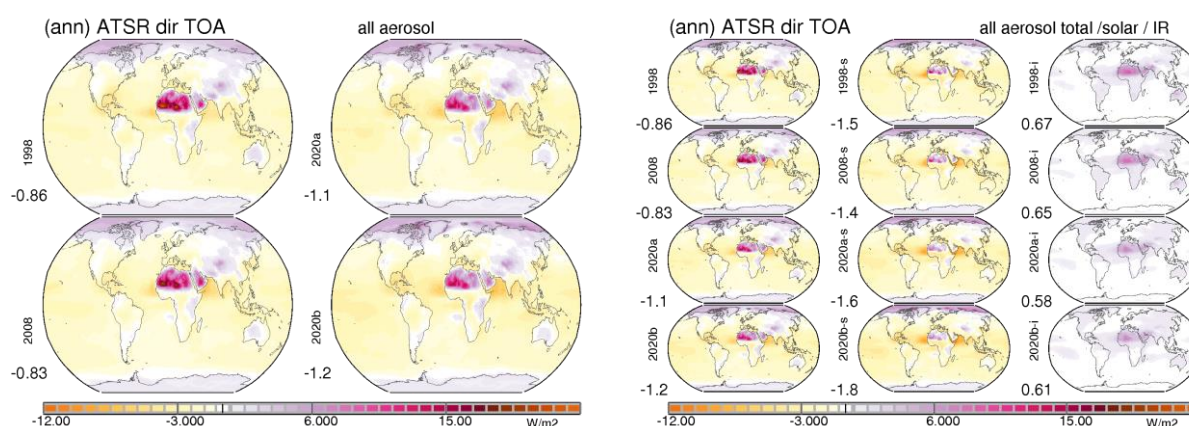


Figure 3.10: Annual global distributions for aerosol direct radiative effects at the top of atmosphere (TOA) (left block) by applying satellite AOD and AODf retrievals of ATSR2 in 1998 (row1), AATSR in 2008 (row2), SLSTR Sentinel-3A (row3) and SLSTR Sentinel-3B (row4) in 2020. Negative values indicate cooling and positive values a warming. Values to the lower left represent global annual averages. Also (right block) totals (col1) are separated into contributions from the solar (col2) and the infrared spectral region (col3).

Total aerosol radiative effects – at surface

The all aerosol direct radiative effect at the surface varies globally between - 5.4 and - 6.4 W/m², with the stronger cooling associated with the most recent SLSTR data. On a regional basis the surface aerosol radiative effects vary between - 40 and 0 W/m², with the strongest cooling over continental regions with (strongly absorbing) wildfire and (absorbing) urban pollution. Aside from reductions to the solar radiation there are also IR re-radiation gains by elevated (colder) dust, so that the reductions of solar radiation over deserts are almost compensated.

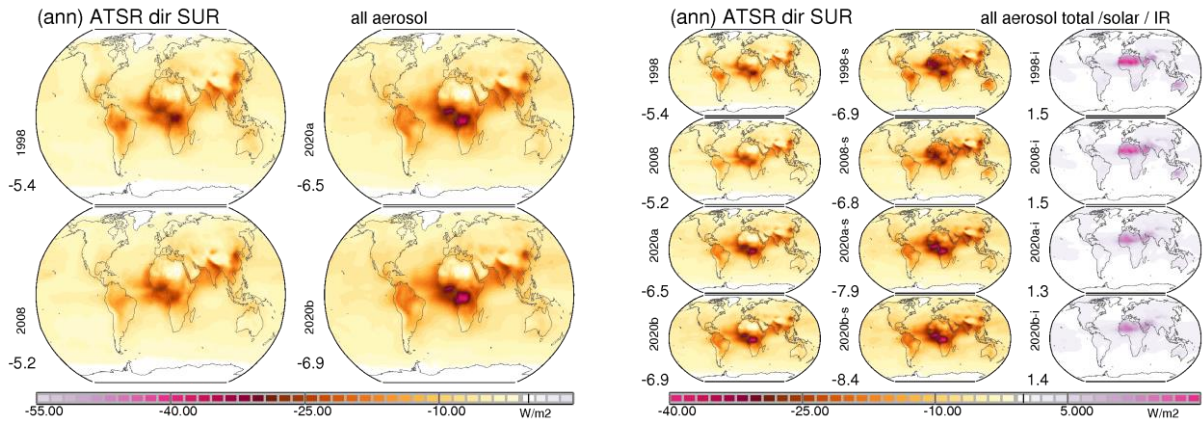


Figure 3.11: Annual global distributions for aerosol direct radiative effects at the (earth) surface (left block) by applying satellite AOD and AODf retrievals of ATSR2 in 1998 (top left), AATSR in 2008 (bottom left) and SLSTR Sentinel-3A (top right) and SLSTR Sentinel-3B (bottom right) in 2020. Negative values indicate that today's aerosol reduces the net radiation at the surface. Values to the lower left represent global annual averages. Also (right block) totals (col1) are separated into contributions from the solar (col2) and the infrared spectral region (col3).

Total aerosol radiative effects – in atmosphere

The direct radiative effect for total aerosol in the atmosphere varies globally between +4.5 and +5.7 W/m², with the strongest solar heating of the aerosol layers by the most recent SLSTR data. The aerosol atmospheric effects are positive and can reach over regions with strong aerosol absorption values in excess of +30 W/m². The strongest solar heating is over biomass region of western Africa in the DJF season and for wildfires over the Congo region in the JJA season.

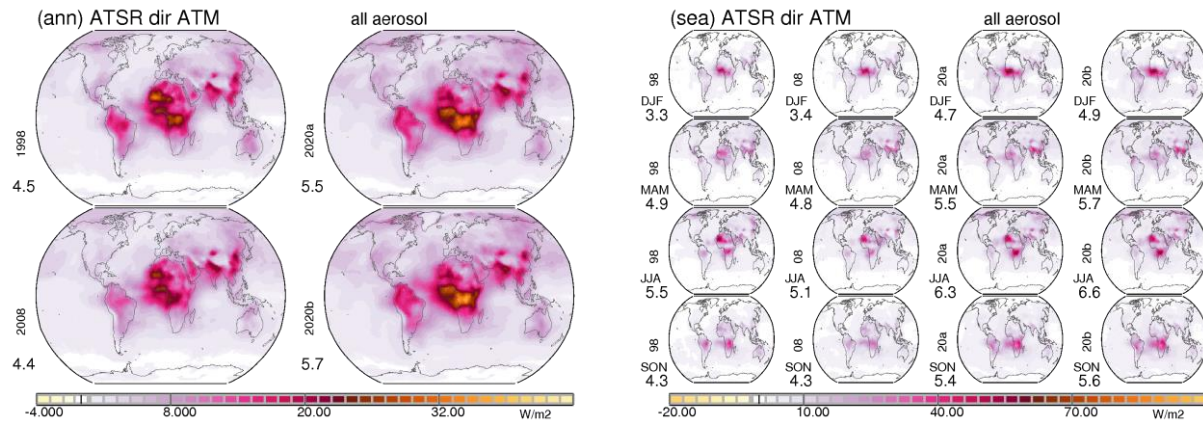


Figure 3.12: Annual (left block) and seasonal (right block) global distributions for aerosol direct radiative (solar heating) effects in the atmosphere by applying satellite AOD and AODf retrievals of ATSR2 in 1998 (top left / col1), AATSR in 2008 (bottom left / col2), SLSTR Sentinel-3A (top right / col3) and SLSTR Sentinel-3B (bottom right / col4) in 2020. Values to the lower left represent global and seasonal annual averages.

Direct aerosol radiative forcing – at TOA

As anthropogenic aerosol in MACv3 is defined as a fraction of the smaller sub-micrometer aerosol sizes (via an AODf fraction from global modeling) there are only solar direct effects. (And even if a small fraction of dust would be as anthropogenic, the dust radiative effects are close to neutral – so that if anthropogenic dust would exist, it would not significantly contribute to an aerosol radiative forcing.)

The direct aerosol forcing (aerosol radiative effects at the TOA at all-sky conditions) varies between - 0.24 and - 0.29 W/m², with the strongest cooling associated with the most recent SLSTR data. Regionally and seasonally the aerosol direct forcing varies between – 6.0 W/m² (pollution outflow offshore, NH urban regions during summer) and +4.0 W/m (absorbing aerosol over snow). Even over oceans there is the SE Atlantic region with small warming during the SON season, when absorbing wildfire aerosols are advected over stratocumulus cloud fields. Overall regions with climate cooling dominate.

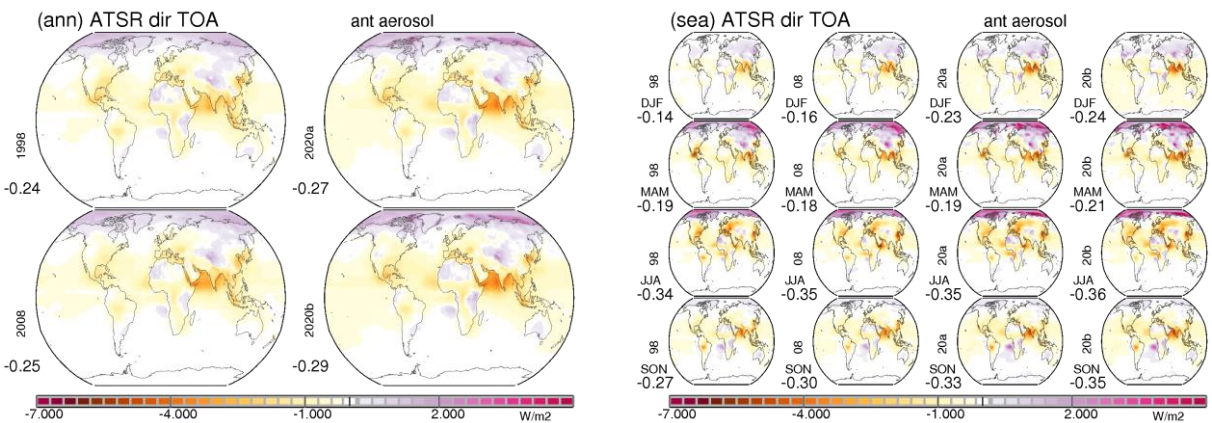


Figure 3.13: Annual (left block) and seasonal (right block) global distributions for direct radiative effects by anthropogenic aerosol at the top of atmosphere (TOA) by applying satellite AOD and AODf retrievals of ATSR2 in 1998 (top left / col1), AATSR in 2008 (bottom left / col2), SLSTR Sentinel-3A (top right / col3) and SLSTR Sentinel-3B (bottom right / col4) in 2020. Values to the lower left represent global and seasonal annual averages.

Anthropogenic aerosol radiative effects – at surface

The direct radiative effects by anthropogenic aerosol at the surface vary globally between - 1.5 and - 1.9 W/m², with the solar radiation reductions associated with the most recent SLSTR data. The surface radiative effect is negative everywhere and can be as large as - 20 W/m². The strongest cooling occurs over continental regions and seasons with (strongly absorbing) wildfire and (absorbing) urban pollution. Maximum solar radiations reductions are over E. Asia during the MAM season and for SLSTR data over the Congo regions during the JJA season.

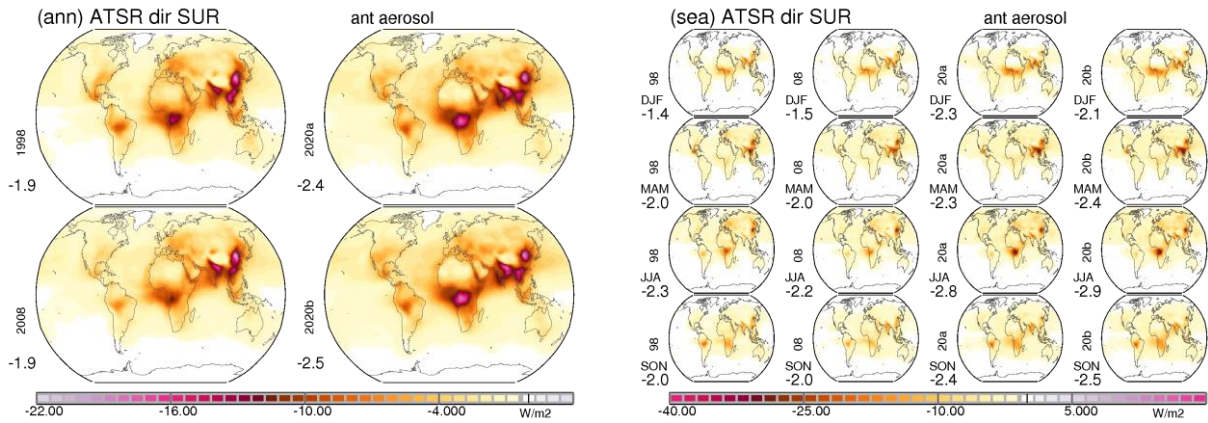


Figure 3.14: annual (left block) and seasonal (right block) global distributions for direct radiative effects by anthropogenic aerosol at the (earth) surface by applying satellite AOD and AODf retrievals of ATSR2 in 1998 (top left / col1), AATSR in 2008 (bottom left / col2), SLSTR Sentinel-3A (top right / col3) and SLSTR Sentinel-3B (bottom right / col4) in 2020. Values to the lower left represent global and seasonal annual averages.

Anthropogenic aerosol radiative effects – in the atmosphere

The direct radiative effects by anthropogenic aerosol in the atmosphere vary globally between +1.7 and +2.2 W/m², with the strongest solar heating of the aerosol layers by the most recent SLSTR data. The aerosol atmospheric effects are positive and can reach over regions with strong aerosol absorption values in excess of +15 W/m². The strongest solar heating is over biomass region of western Africa in the DJF season, over East Asia (with bright lower clouds) during the MAM season, for wildfires over the Congo region in the JJA season and over wildfire regions of South Africa and South America during the SON dry season.

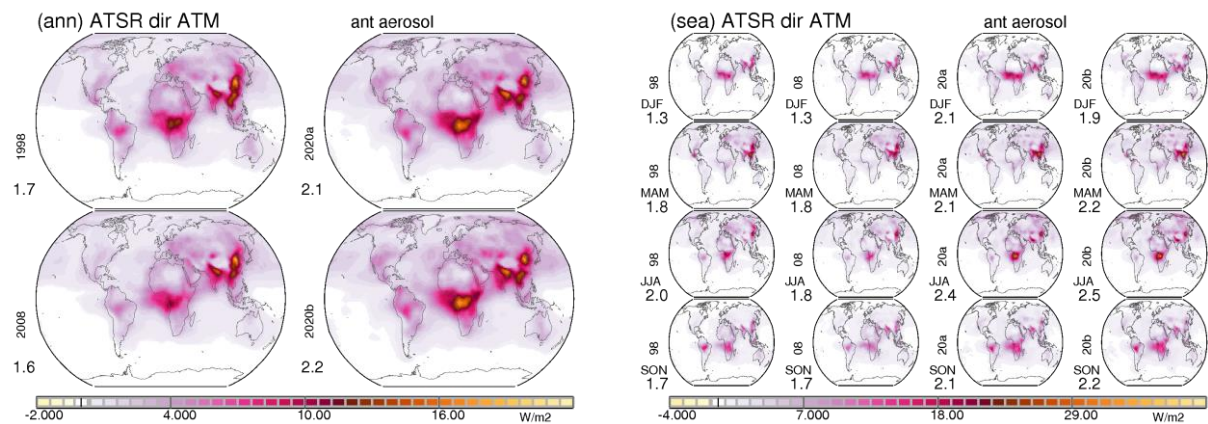


Figure 3.15: annual (left block) and seasonal (right block) global distributions for direct radiative (solar heating) effects by anthropogenic aerosol in the atmosphere by applying satellite AOD and AODf retrievals of ATSR2 in 1998 (top left / col1), AATSR in 2008 (bottom left / col2), SLSTR Sentinel-3A (top right / col3) and SLSTR Sentinel-3B (bottom right / col4) in 2020. Values to the lower left represent global and seasonal annual averages.



Total (direct and indirect) aerosol radiative forcing – at TOA

The indirect radiative effect by anthropogenic aerosol focuses on the first indirect effect (or Twomey effect). Other associated secondary effects, such as increased lifetime under high humidity conditions and increased evaporation at low humidity conditions are assumed to cancel and are not considered. Thus, only droplet size reductions of water clouds, without changes to the cloud water content are considered. Smaller droplets increase the cloud's planetary albedo and at the same time reduce the solar radiation reaching the surface. Extra solar heating by a modified cloud is very small compared to the solar heating by the aerosol direct effect and - due to the near surface location of water clouds - infrared effects from increased cloud optical depths are minor.

The combined direct and indirect aerosol forcing (aerosol radiative effects at the TOA at all-sky conditions) varies between is almost identical at -0.87 W/m^2 . Regionally and seasonally the combined (direct and indirect) anthropogenic forcing varies between -6.0 and $+2.0 \text{ W/m}^2$. Compared to the direct forcing the cooling over urban regions and over (dark) oceanic regions with pollution outflow is increased. The JJA season contributes with the strongest cooling.

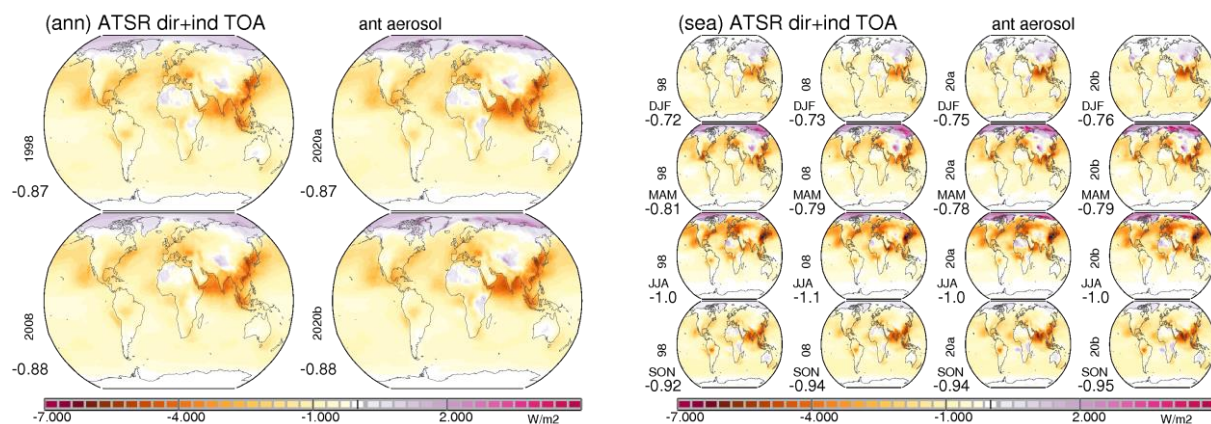


Figure 3.16: annual (left block) and seasonal (right block) global distributions for direct and indirect radiative effects by anthropogenic aerosol at the top of atmosphere (TOA) by applying satellite AOD and AODf retrievals of ATSR2 in 1998 (top left / col1), AATSR in 2008 (bottom left / col2), SLSTR Sentinel-3A (top right / col3) and SLSTR Sentinel-3B (bottom right / col4) in 2020. Values to the lower left represent global and seasonal annual averages.

Total (direct and indirect) anthropogenic aerosol radiative effect – at the surface

The combined direct and indirect radiative effects by anthropogenic aerosol at the surface vary globally between -2.6 and -3.1 W/m^2 , with the larger solar radiation reductions associated with the SLSTR data. The surface radiative effect is negative everywhere and can be as large as -20 W/m^2 . Compared to the direct impact, mainly the cooling over oceans with pollution outflow is increased.

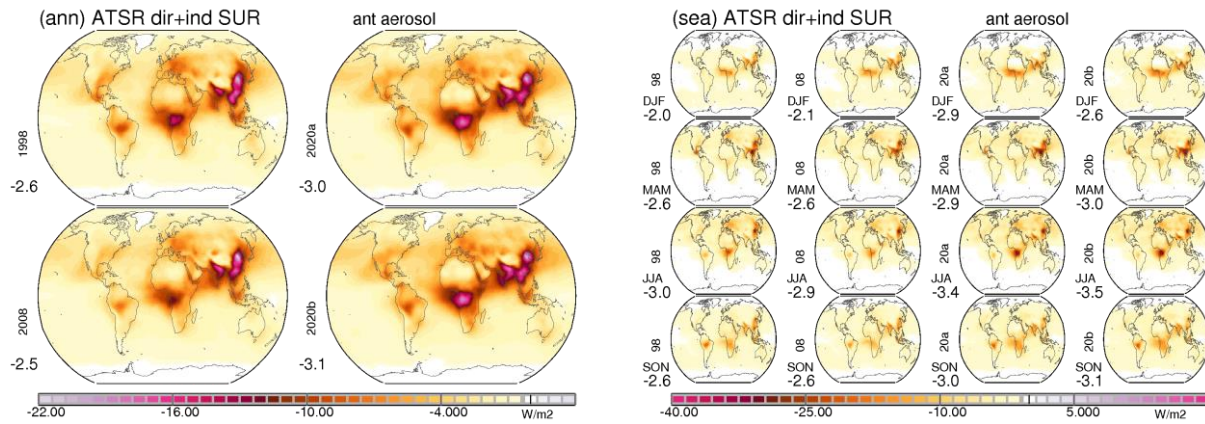



Figure 3.17: annual (left block) and seasonal (right block) global distributions for direct and indirect radiative effects by anthropogenic aerosol at the (earth) surface by applying satellite AOD and AODf retrievals of ATSR2 in 1998 (top left / col1), AATSR in 2008 (bottom left / col2), SLSTR Sentinel-3A (top right / col3) and SLSTR Sentinel-3B (bottom right / col4) in 2020. Values to the lower left represent global and seasonal annual averages.

	Aerosol_cci+ Climate Assessment Report	REF : aerosol CAR ISSUE : 3.1 DATE : 19.07.2022 PAGE : 20
---	---	--

4 DATA ASSIMILATION

Overview of the user case study

In recent years significant progress of the CAMS modeling system has led to significant improvements of the modelling system and thus shown only weak impact of assimilating MODIS AOD (except for episodic high AOD cases such as autumn biomass burning). Therefore, expectations for the SLSTR AOD assimilation test remained realistic, while future potential lies in exploiting more information than just AOD (e.g. PM at the surface, absorption SSA or AAOD, Fine Mode AOD) for verification or assimilation. MODIS assimilation proved more valuable where AERONET station density is low but also had still positive impact over Europe. In order to quantify the impact of SLSTR data, the assimilation user case study focused on assessing and separating potential cases of high Aerosol_cci+ dataset impact (e.g. biomass burning events).

The study used level 2 data for the full month of September 2019 when the biomass burning signal is strongest.

Assimilation experiments with ECMWF's IFS in the CAMS configuration were then performed using Aerosol Optical Depth. Four one-month experiments were conducted:

- a control experiments without any aerosol data in the assimilation
- one experiment with only SLSTR data
- one experiment with all other available AOD data (MODIS, PMAP) excluding SLSTR
- one experiment with all available data including SLSTR.

The impact of the various datasets was assessed using the standard AERONET verification which is applied operationally in CAMS. Specific AERONET stations and regions were looked at in more detail to understand the regional impact of the SLSTR dataset and its strength/weaknesses with respect to the other datasets.

Initial light dataset evaluation for this user case study / 2019 datasets Swansea algorithm

One year of level-3 SLSTR SU v1.14 S3A and S3B Aerosol Optical Depth (AOD) monthly mean data were assessed. Qualitative comparisons were performed against AOD from the CAMS reanalysis (Inness, et al 2019). The agreement is generally good, although there are some differences highlighted below, month by month (Figures 4.1 – 4.12).

In January it is possible to see that the SLSTR AOD data show lower values over India and China whereas the biomass burning regions of Central Africa show values of AOD higher than the CAMS reanalysis. The global average for S3A is lower than S3B, but overall there is a large degree of consistency between the two SLSTR instruments. Both satellite datasets show a 30% difference in global average AOD. A similar behaviour is identifiable for the month of February 2019.

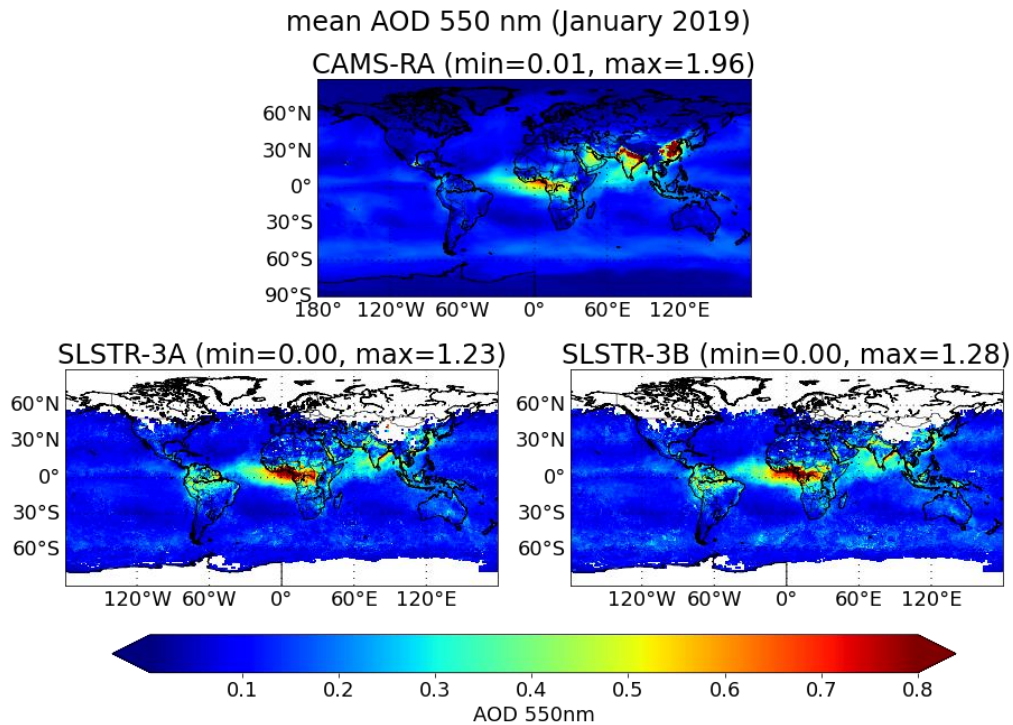
	Aerosol_cci+ Climate Assessment Report	REF : aerosol CAR ISSUE : 3.1 DATE : 19.07.2022 PAGE : 21
---	---	--

In March 2019, both SLSTR AOD data show a larger contribution over China which seems to agree better with the CAMS reanalysis. The signal from central Africa is still larger in the SLSTR AOD than in the CAMS reanalysis. Over the Arabian Peninsula, however, the opposite is true. A similar behaviour is observed in April. In May good similarities are observed for AOD over the Sahara and generally East Asia. Central America also displays similar features between the three datasets.

In June, more dust signal is observed in the SLSTR datasets than in the CAMS reanalysis. Also, some high latitude high AOD episodes, possibly related to boreal fires, are visible in the SLSTR, but not to the same extent in the CAMS reanalysis. Overall, however, the global average for AOD remains lower for the satellite product than for the reanalysis. In July, the signal from the boreal forest fires is more pronounced in the CAMS reanalysis than the SLSTR datasets with patchy large AOD values at high latitudes. The dust signal over the Sahara is instead more pronounced in the SLSTR AOD than in the CAMS reanalysis AOD. The comparisons in August show a good degree of similarities, particularly in the Central Africa biomass burning and Indian Ocean dust signal. The latter is also very strong in July.

In September, the main features are the biomass burning in South America, Africa and Indonesia, well visible in all three datasets. For Central and East Asia, the AOD signal is larger in the SLSTR datasets than in the CAMS reanalysis. This continues into the month of October. The large AOD associated to biomass burning in Indonesia is well captured in all three datasets and persists into October. The month of November shows the worst agreement with large values of AOD in South America that are not captured by the reanalysis. Vice versa, the signal of anthropogenic aerosols over India and China is much lower in the SLSTR datasets than in the CAMS reanalysis. The global average for the CAMS reanalysis is more than double that of the SLSTR AOD datasets. A similar situation is visible in December. A general good agreement over Australia due to the signal of the bush fires is visible both in November and in December.

(a)



(b)

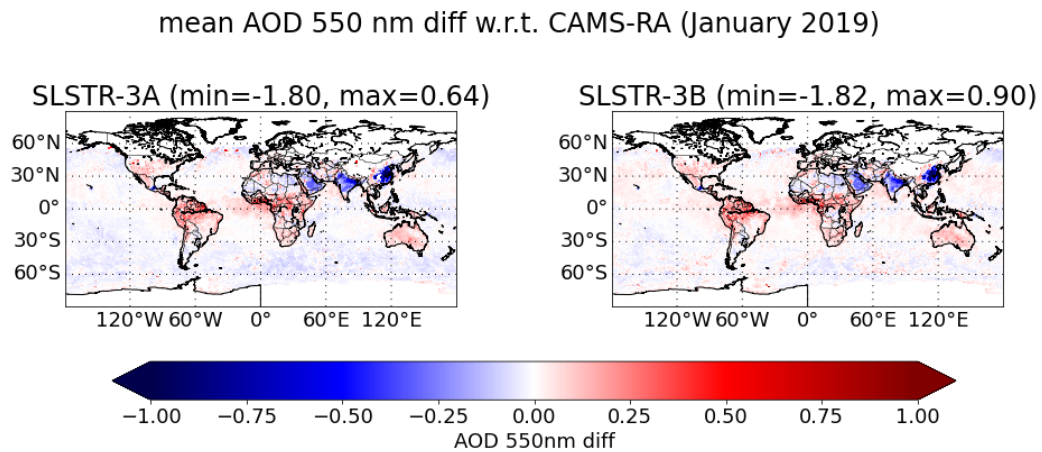
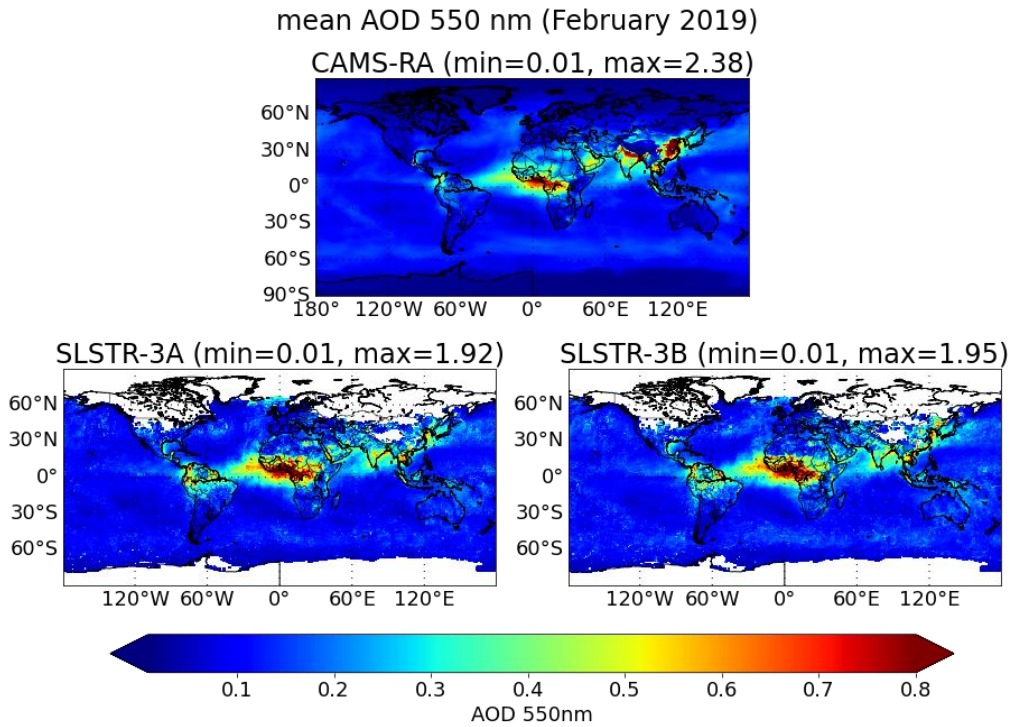


Figure 4.1 (a) AOD comparisons for the month of January 2019: CAMS reanalysis (top panel), SLSTR SU product from Sentinel 3A (left) and SLSTR SU product from Sentinel 3B (right); (b) absolute difference between SLSTR-S3A and S3B with respect to the CAMS analysis.

(a)



(b)

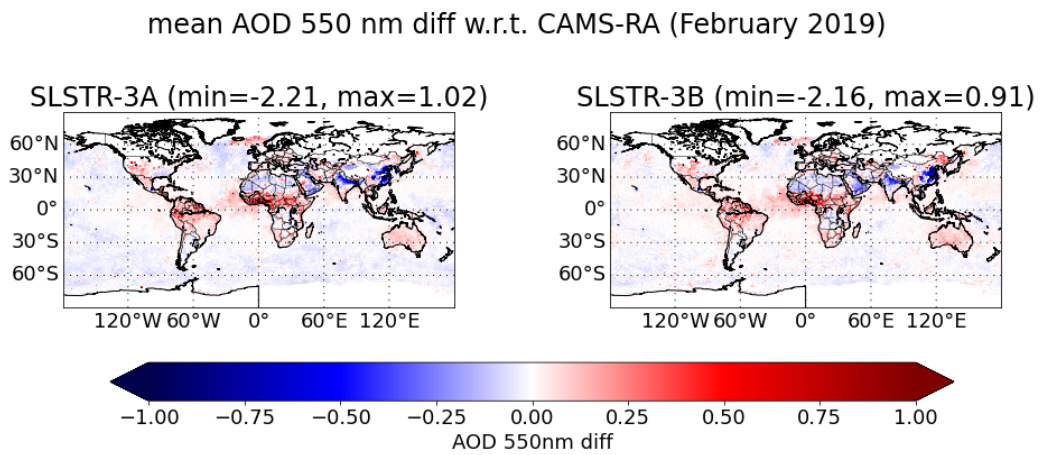
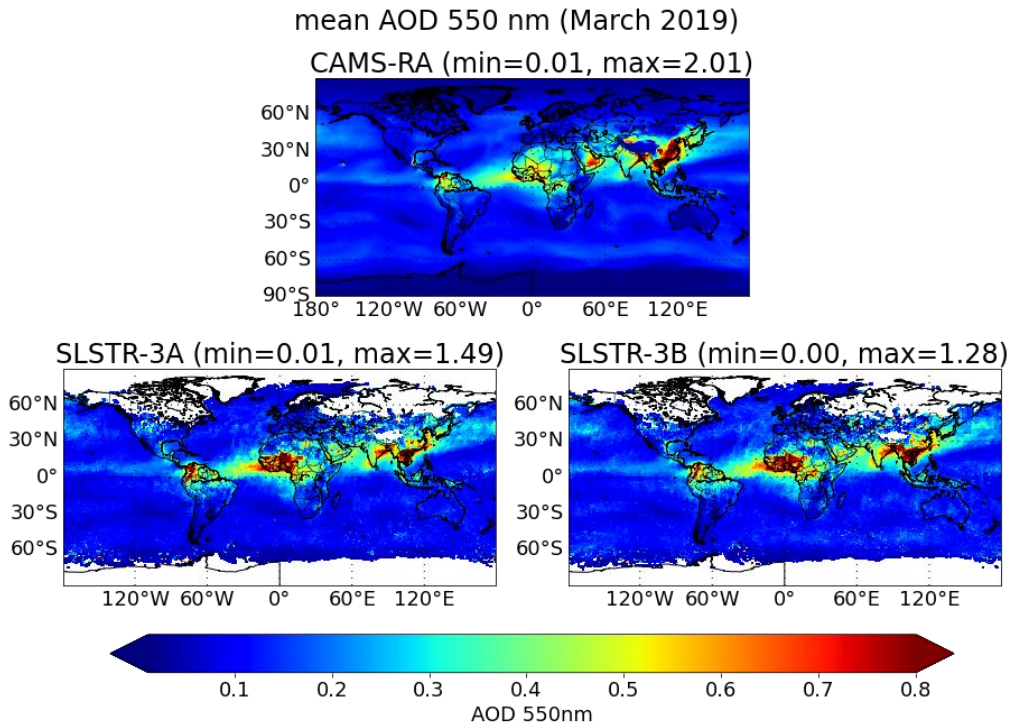


Figure 4.2 Same as figure 4.1 but for February 2019.

(a)



(b)

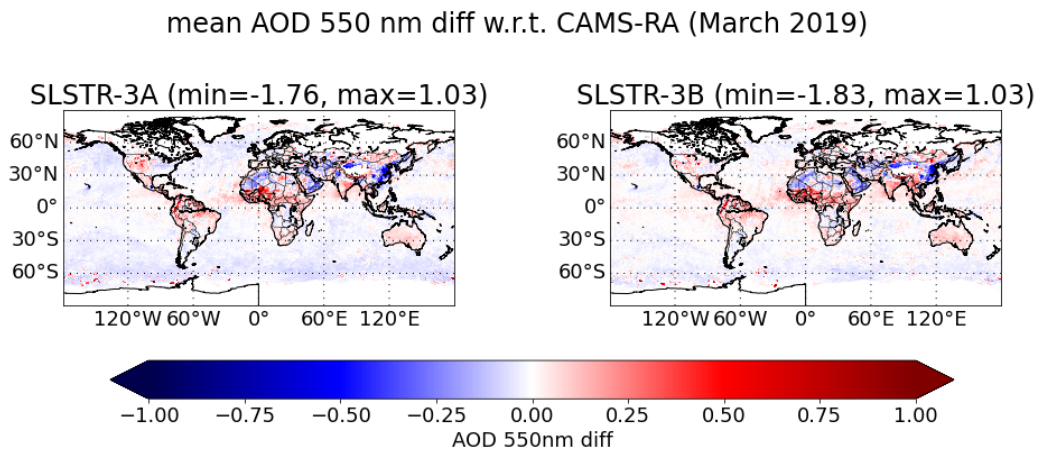
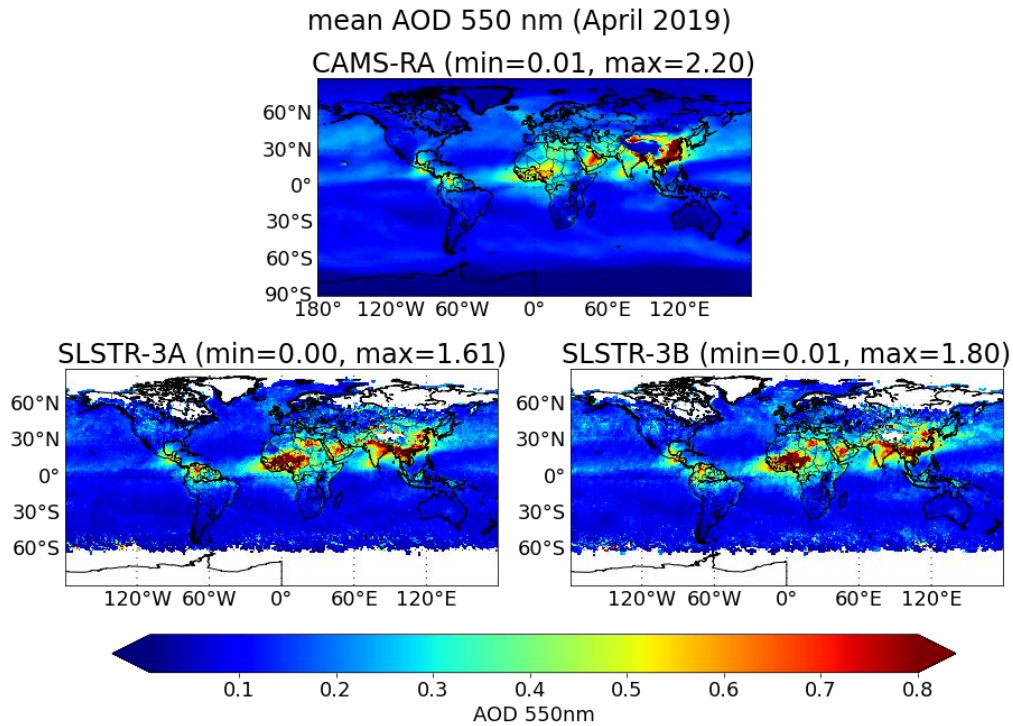


Figure 4.3 Same as figure 4.1 but for March 2019.

(a)



(b)

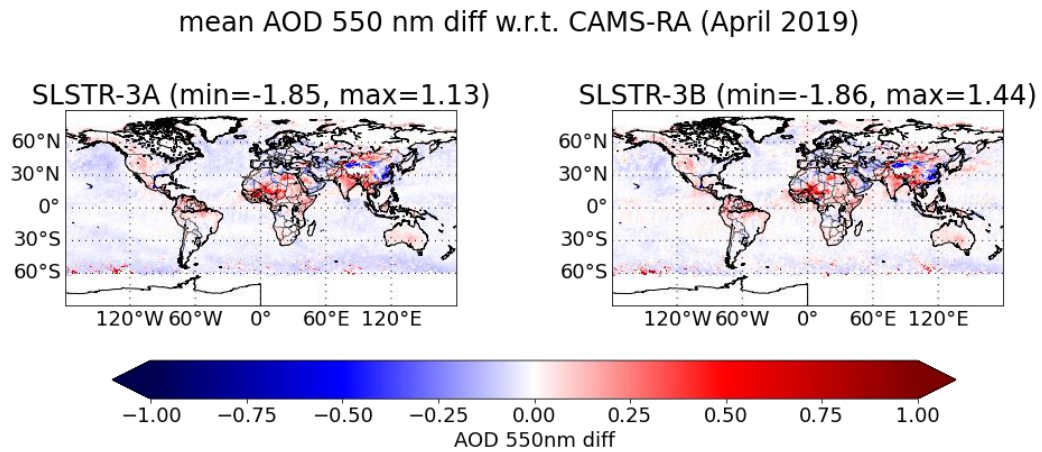
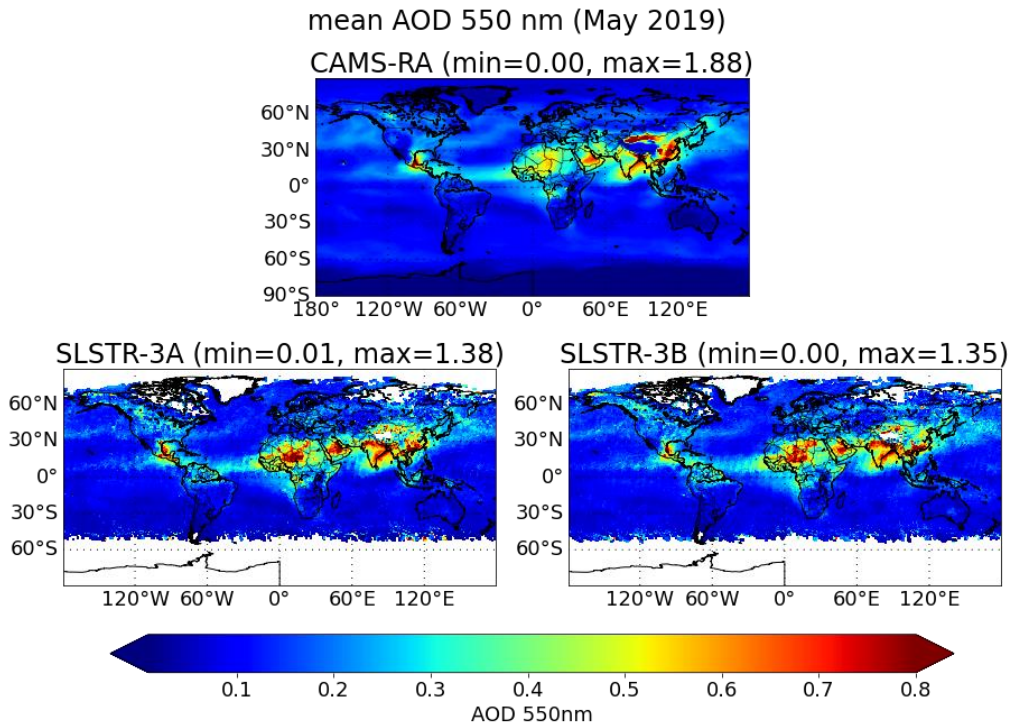


Figure 4.4 Same as figure 4.1 but for April 2019.

(a)



(b)

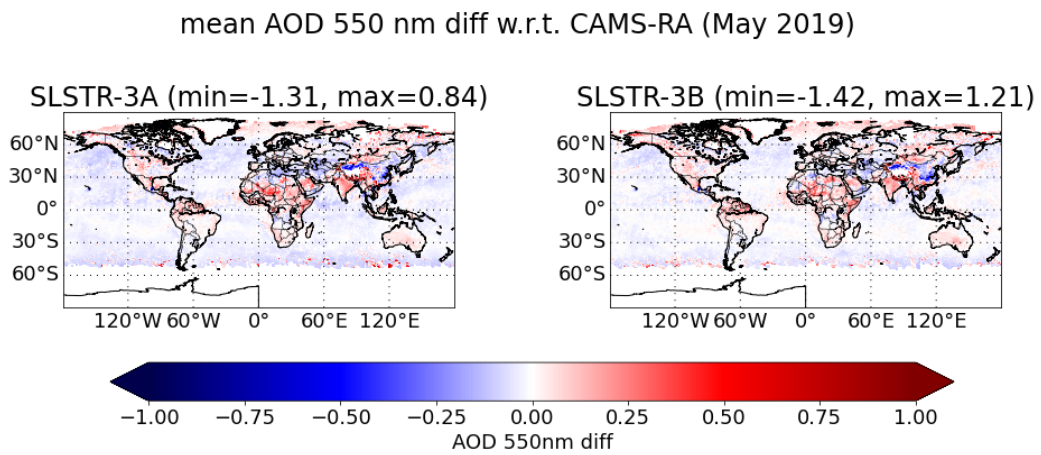
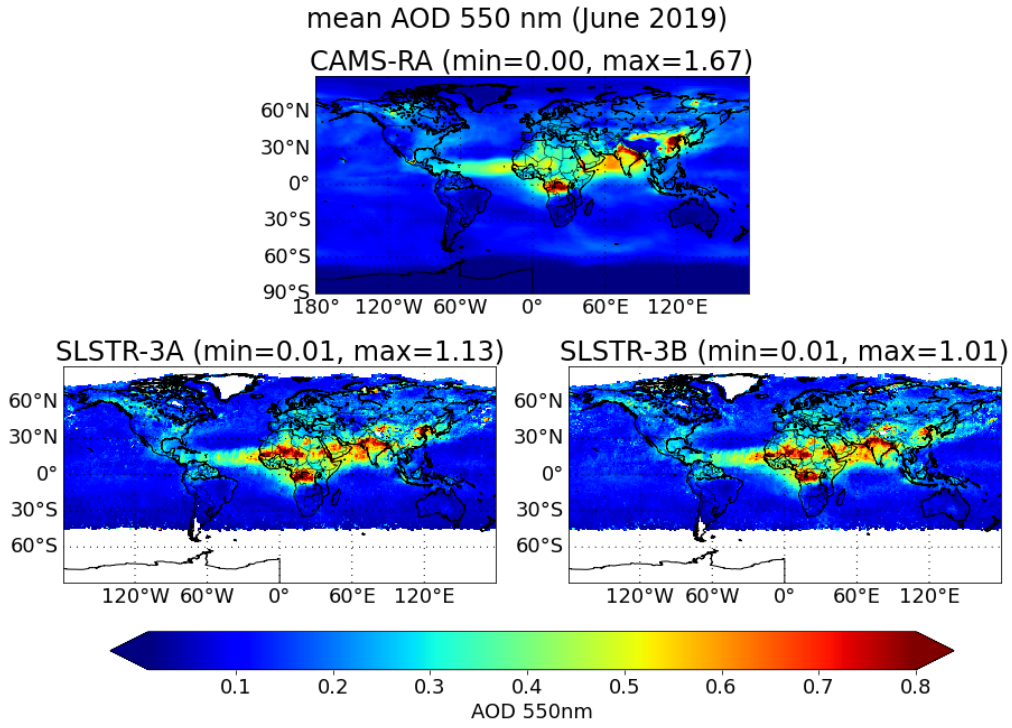


Figure 4.5 Same as figure 4.1 but for May 2019.

(a)



(b)

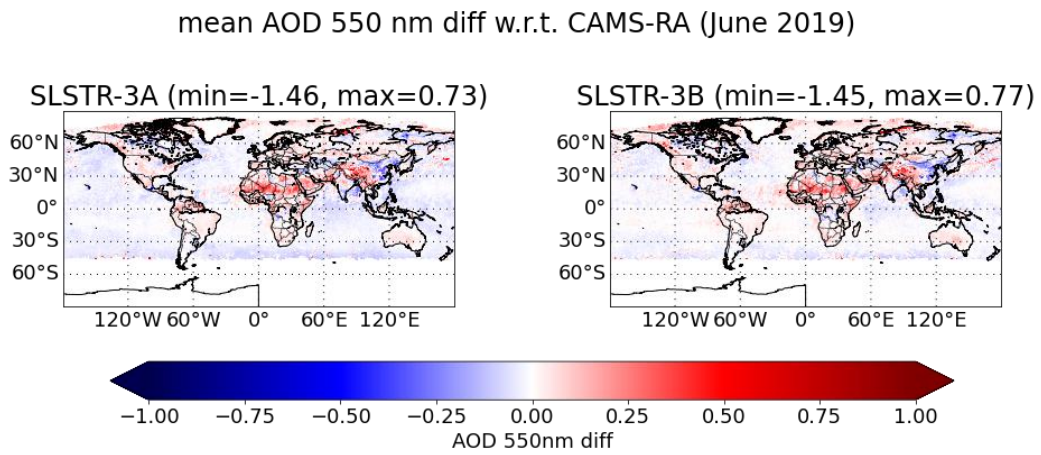
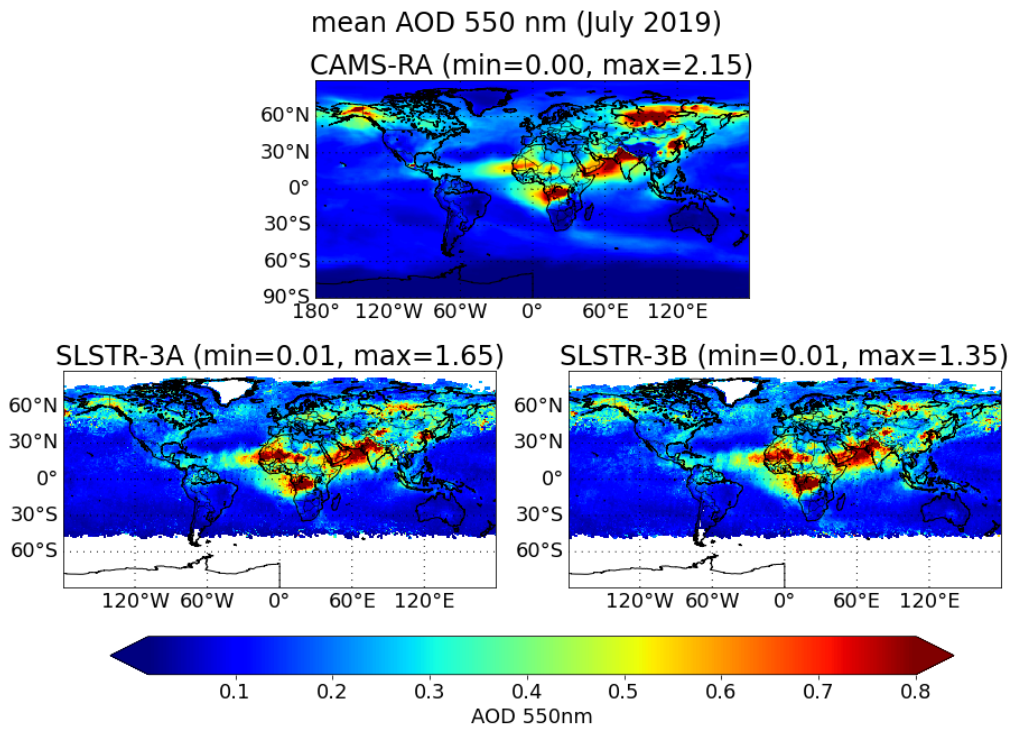


Figure 4.6 Same as figure 4.1 but for June 2019.

(a)



(b)

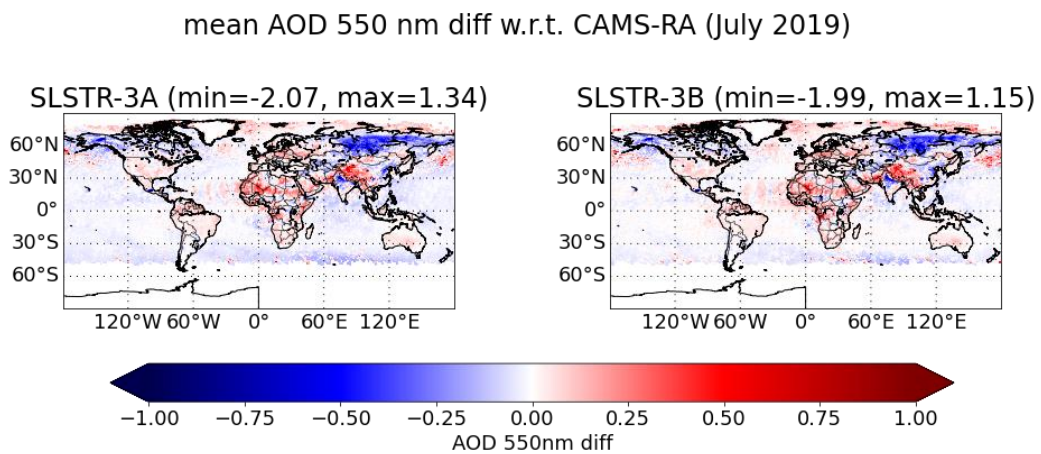
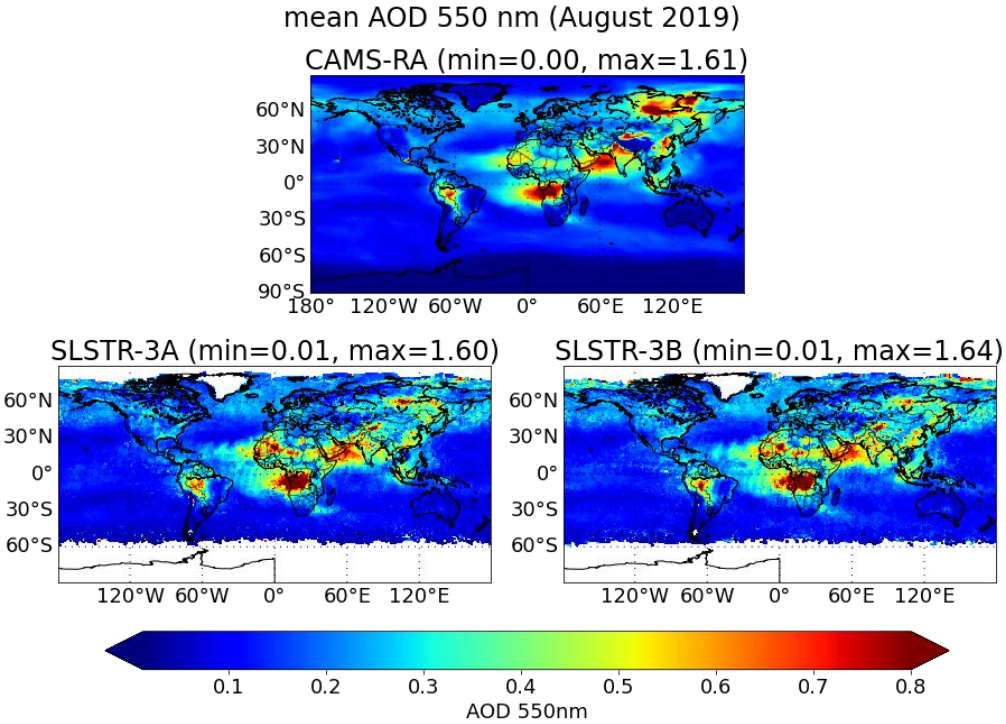


Figure 4.7 Same as figure 4.1 but for July 2019.

(a)



(b)

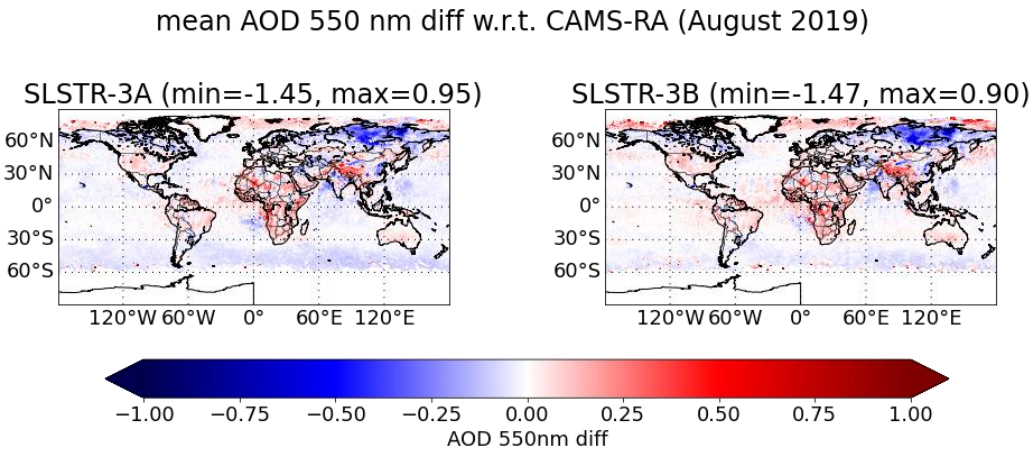
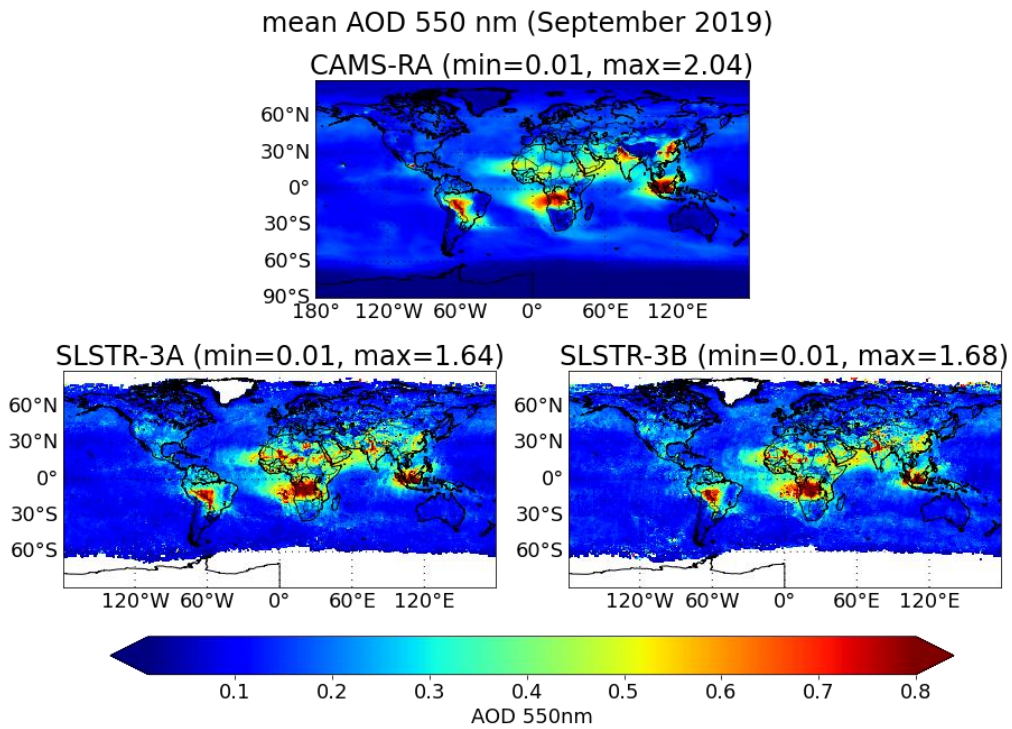


Figure 4.8 Same as figure 4.1 but for August 2019.

(a)



(b)

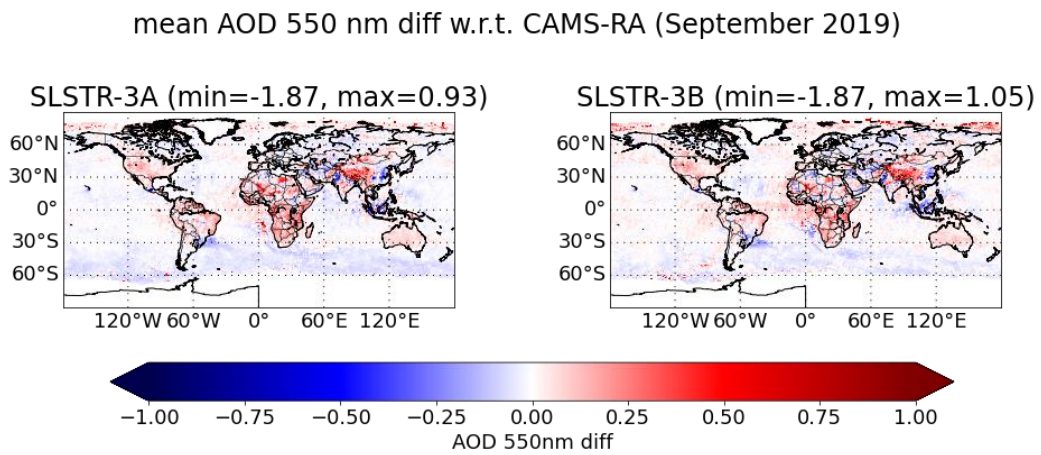
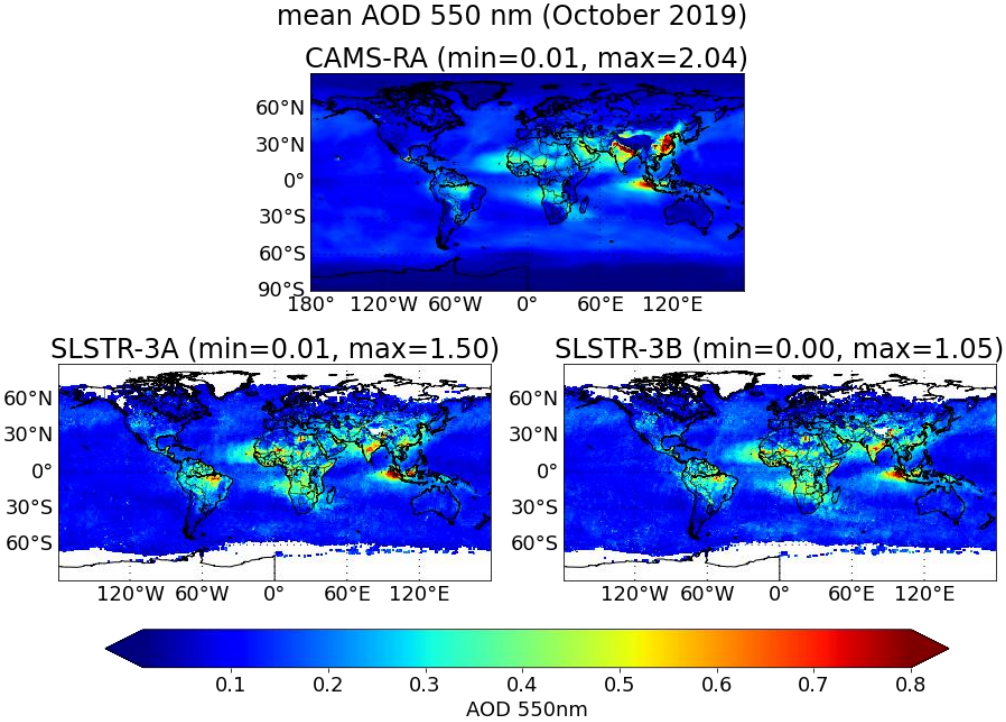


Figure 4.9 Same as figure 4.1 but for September 2019.

(a)



(b)

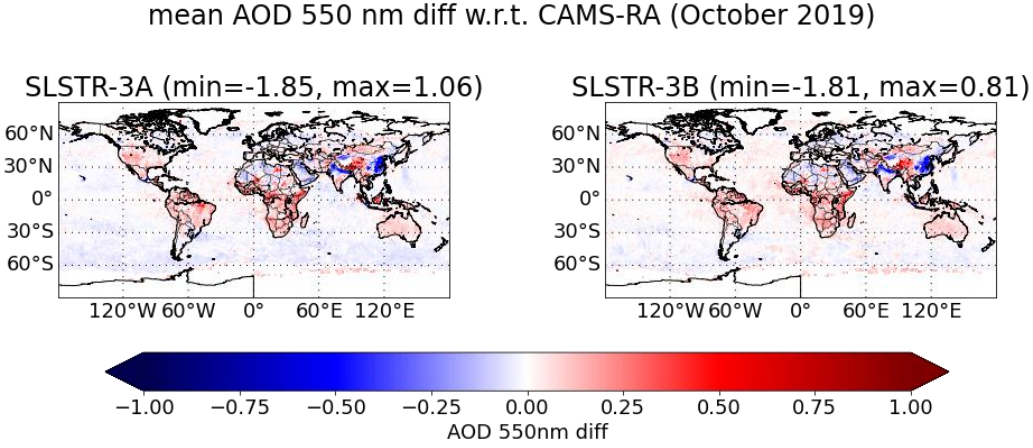
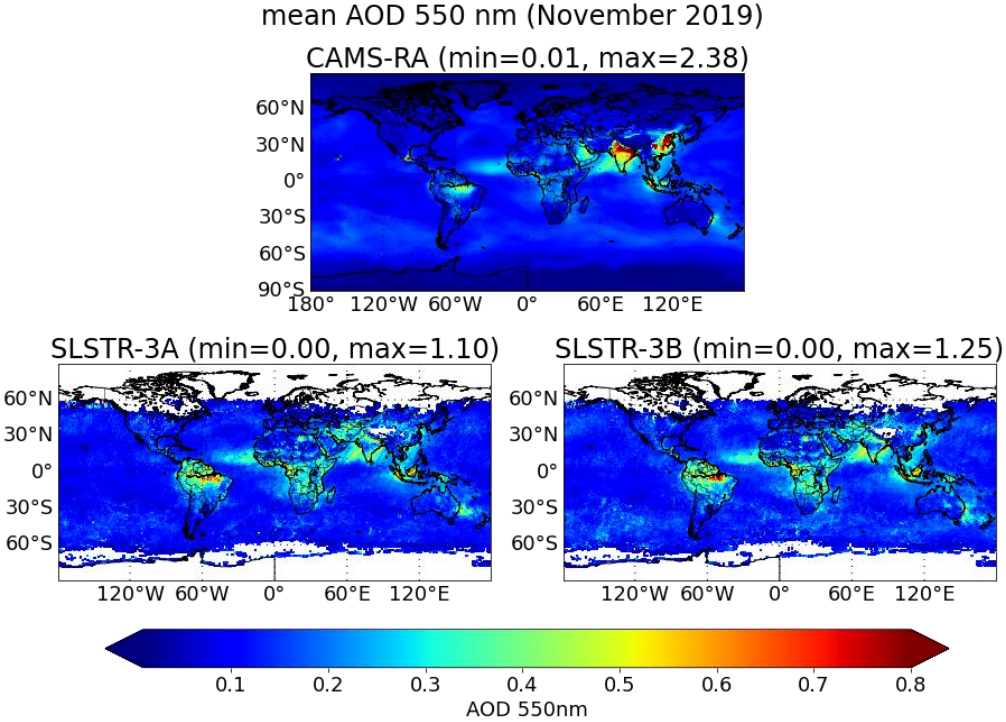


Figure 4.10. Same as figure 4.1 but for October 2019.

(a)



(b)

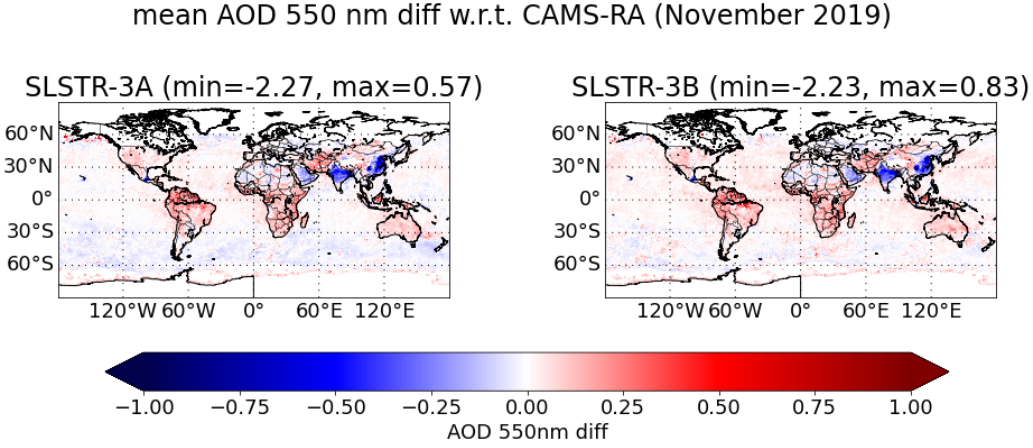
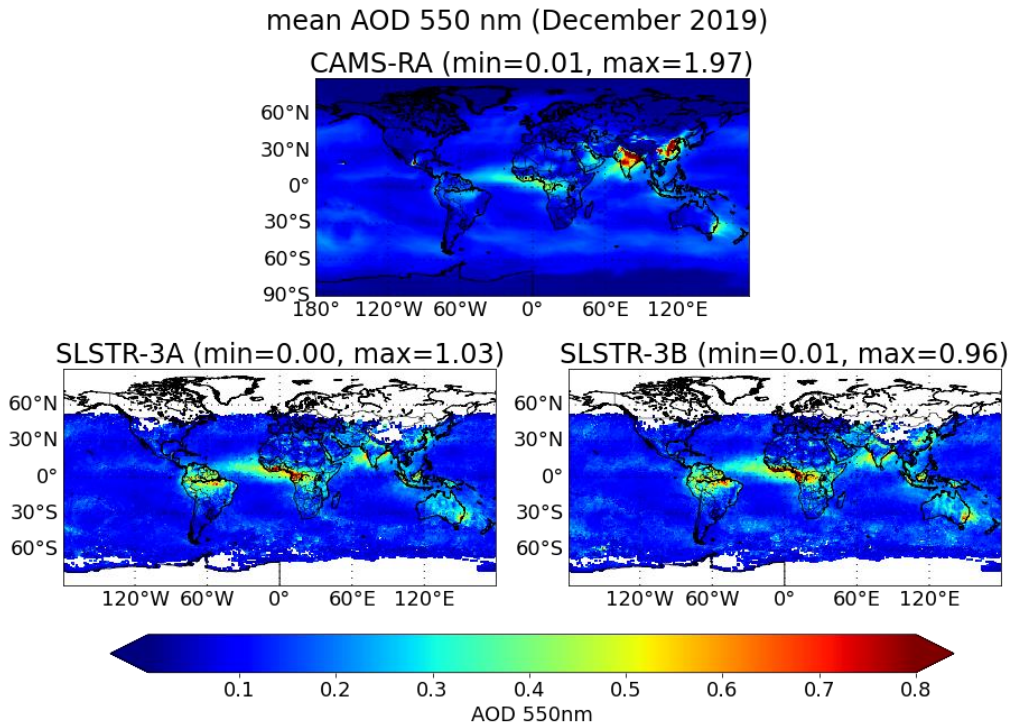


Figure 4.11 Same as figure 4.1 but for November 2019.

(a)



(b)

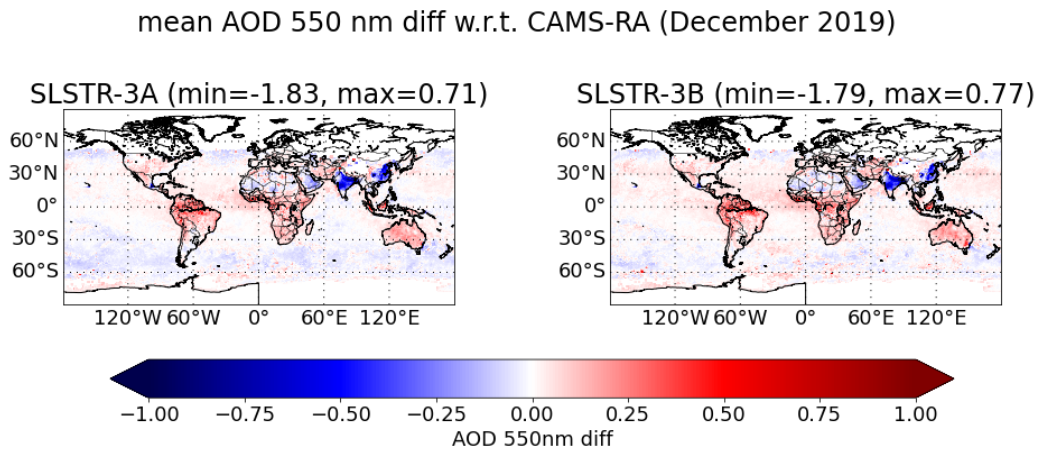


Figure 4.12 Same as figure 4.1 but for December 2019.

Qualitative comparisons with the CAMS reanalysis for 2020 (SU and RF datasets)

One year of level-3 SU SLSTR S3A and S3B v1.14 and Rayference CISAR SLSTR-3A V2.2.1 Aerosol Optical Depth (AOD) monthly mean data were assessed. Qualitative comparisons were performed against AOD from the CAMS reanalysis (Inness, et al 2019). The agreement is generally good for the SU S3A and S3B datasets, although there are some differences highlighted below month by month (Figures 4.13– 4.24). The figures show both absolute values and differences. The largest differences are observed with the Rayference product, also shown in the figures which seems to consistently underestimate AOD, even if the max value of AOD is larger than the corresponding SU SLSTR max value and hence closer to the CAMS reanalysis. Some aerosol features are entirely missing in the CISAR AOD dataset.

In January it is possible to see that the signature of the Australian bush fires in both the SU SLSTR AOD data and the CAMS reanalysis. Generally the retrieval show lower values over India and China whereas the biomass burning regions of Central Africa show values of AOD higher than the CAMS reanalysis, as already observed for 2019. A similar behaviour is identifiable for the month of February 2020.

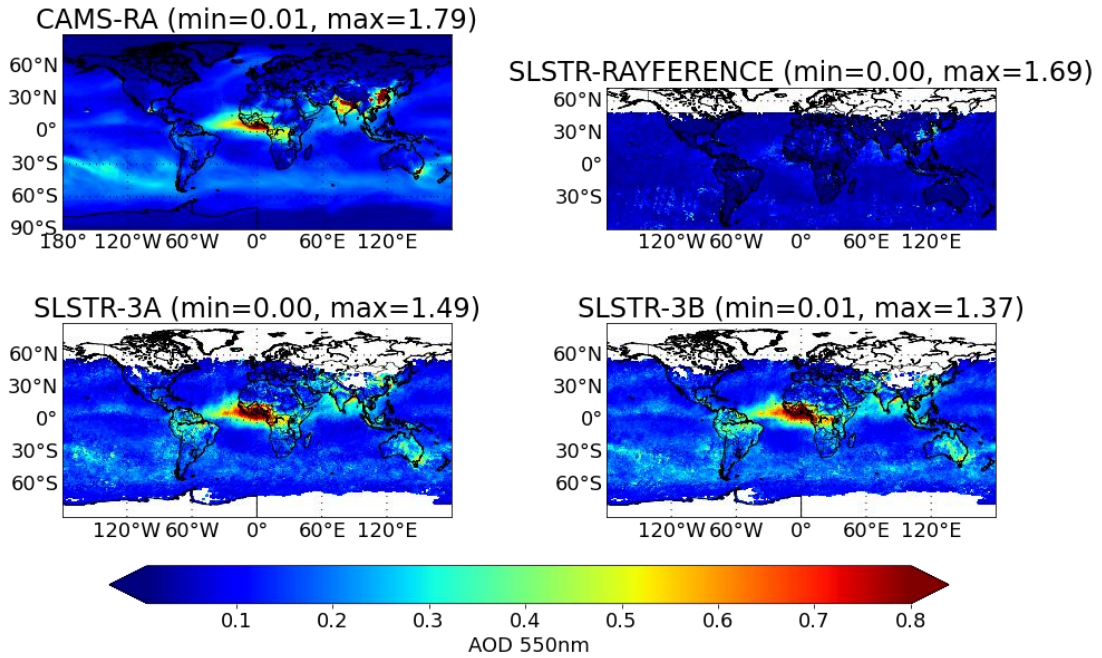
In March 2020, both SLSTR AOD data show a larger contribution over China which seems to agree better with the CAMS reanalysis. The signal from central Africa is still larger in the SLSTR AOD than in the CAMS reanalysis. Values over the Arabian Peninsula, however, are more consistent between the three datasets than for March 2019. A similar behaviour is observed in April. In May and June good similarities are observed for AOD over the Sahara and generally East Asia. Central America also displays similar features between the three datasets.

In July, more dust signal is observed in the SLSTR datasets than in the CAMS reanalysis. Opposite to 2019, the signal from the boreal forest fires is more pronounced in the SLSTR datasets than in the CAMS reanalysis with patchy large AOD values at high latitudes. The comparisons in August show a good degree of similarities, particularly in the Central Africa biomass burning and Indian Ocean dust signal. The latter is also very strong in July.

In September, the main features are the biomass burning in South America and Africa, well visible in all three datasets. Also visible in all three datasets, is the Californian fires signal, although more pronounced in the CAMS reanalysis. Compared to 2019 the signal of the biomass burning season in Indonesia is not as strong. The large AOD values associated to biomass burning in South America persist into October. For the month of November, the signal of anthropogenic aerosols over India and China is much lower in the SLSTR datasets than in the CAMS reanalysis similarly to 2019. A similar situation is visible in December. However, the signal of biomass burning in Central Africa is higher for the SLSTR AOD datasets than the CAMS reanalysis.

(a)

mean AOD 550 nm (January 2020)



(b)

mean AOD 550 nm diff w.r.t. CAMS-RA (January 2020)

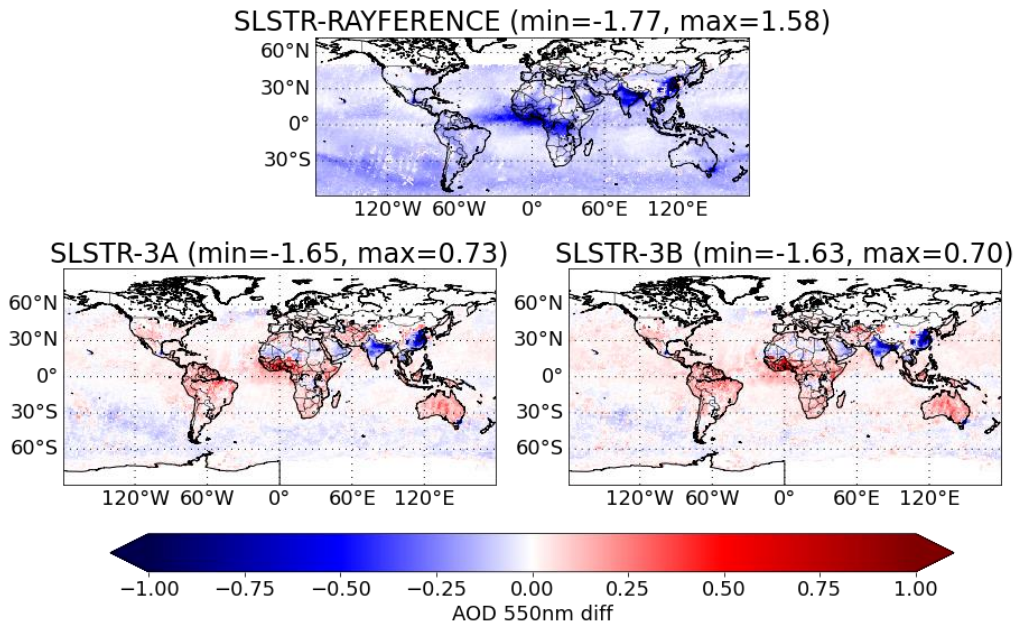
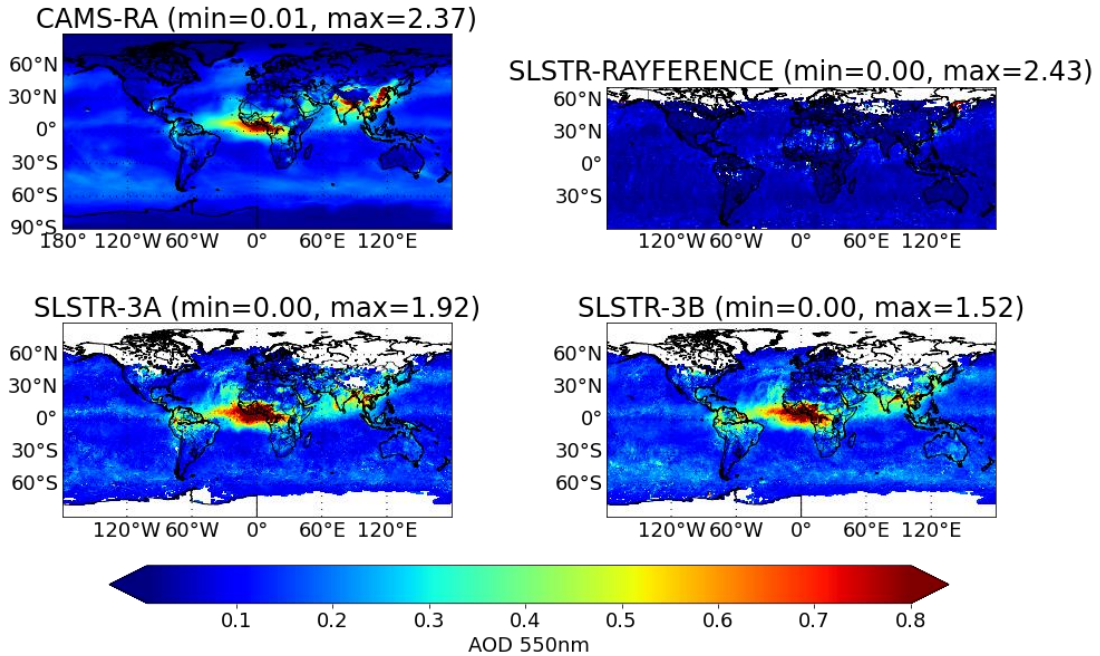


Figure 4.13 (a) AOD comparisons for the month of January 2020: CAMS reanalysis (top left), SLSTR CISAR (top right) SLSTR SU product from Sentinel 3A (bottom left) and SLSTR SU product from Sentinel 3B (bottom right); (b) absolute differences between the satellite datasets and the CAMS reanalysis.

(a)

mean AOD 550 nm (February 2020)



(b)

mean AOD 550 nm diff w.r.t. CAMS-RA (February 2020)

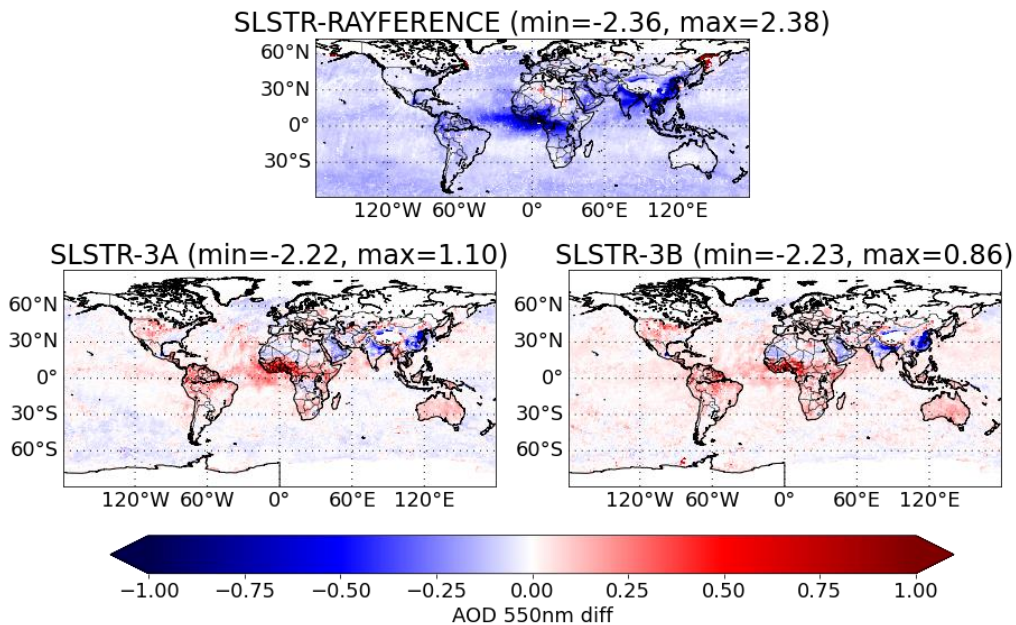
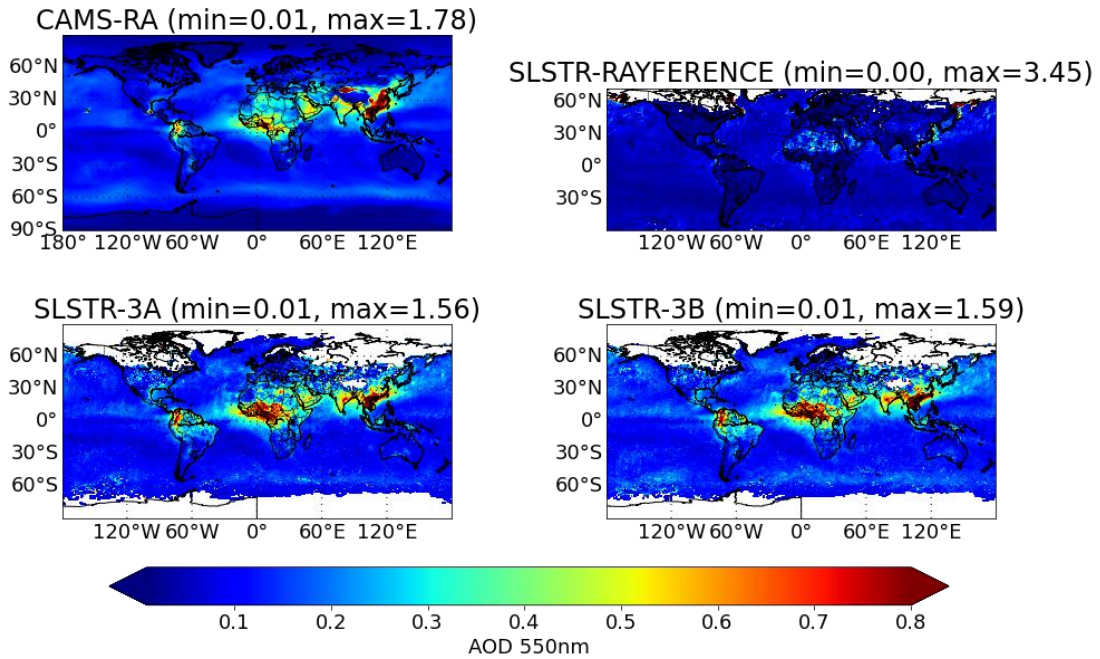


Figure 4.14 Same as figure 4.13 but for February 2020.

(a)

mean AOD 550 nm (March 2020)



(b)

mean AOD 550 nm diff w.r.t. CAMS-RA (March 2020)

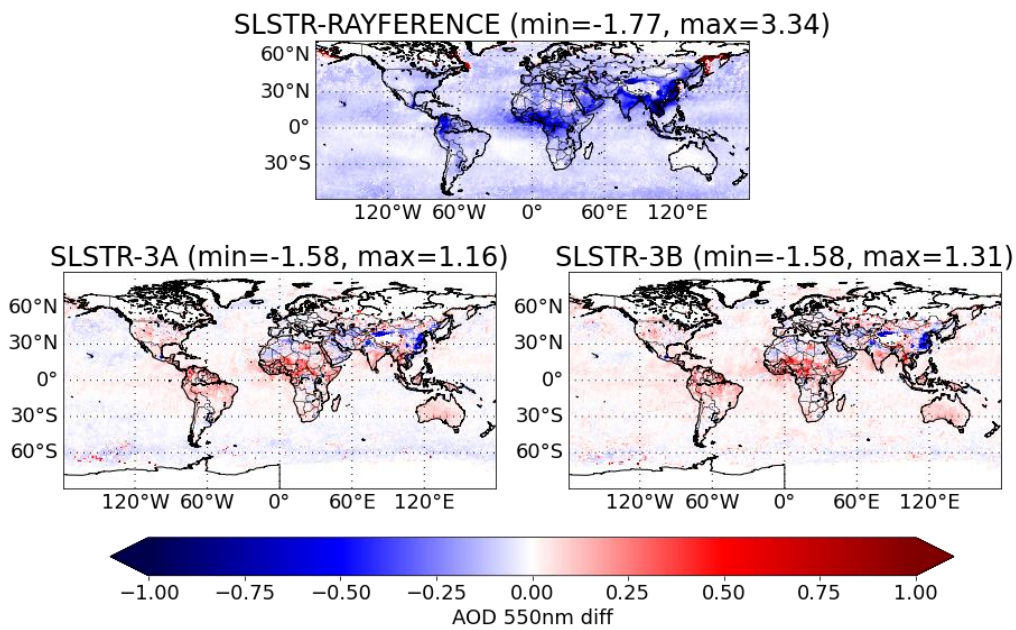
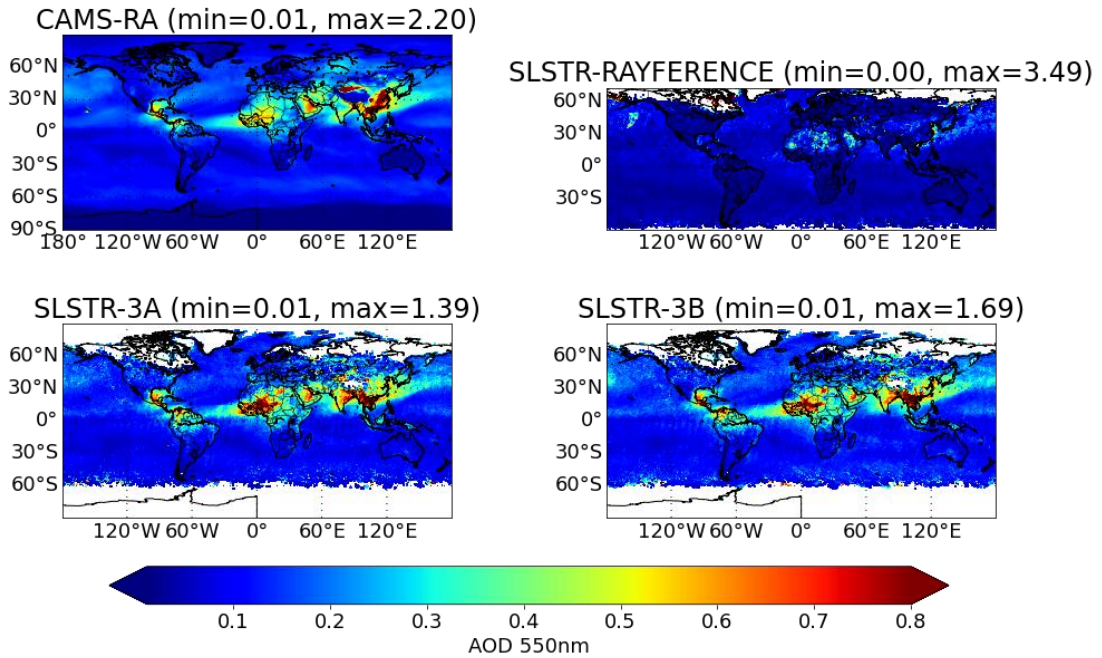


Figure 4.15 Same as figure 4.13 but for March 2020.

(a)

mean AOD 550 nm (April 2020)



(b)

mean AOD 550 nm diff w.r.t. CAMS-RA (April 2020)

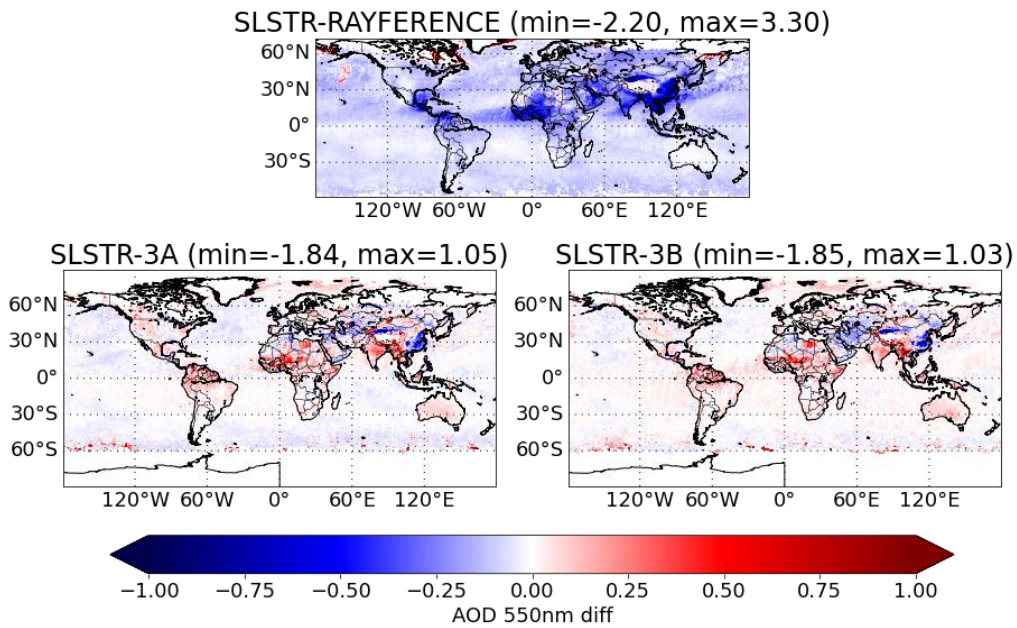
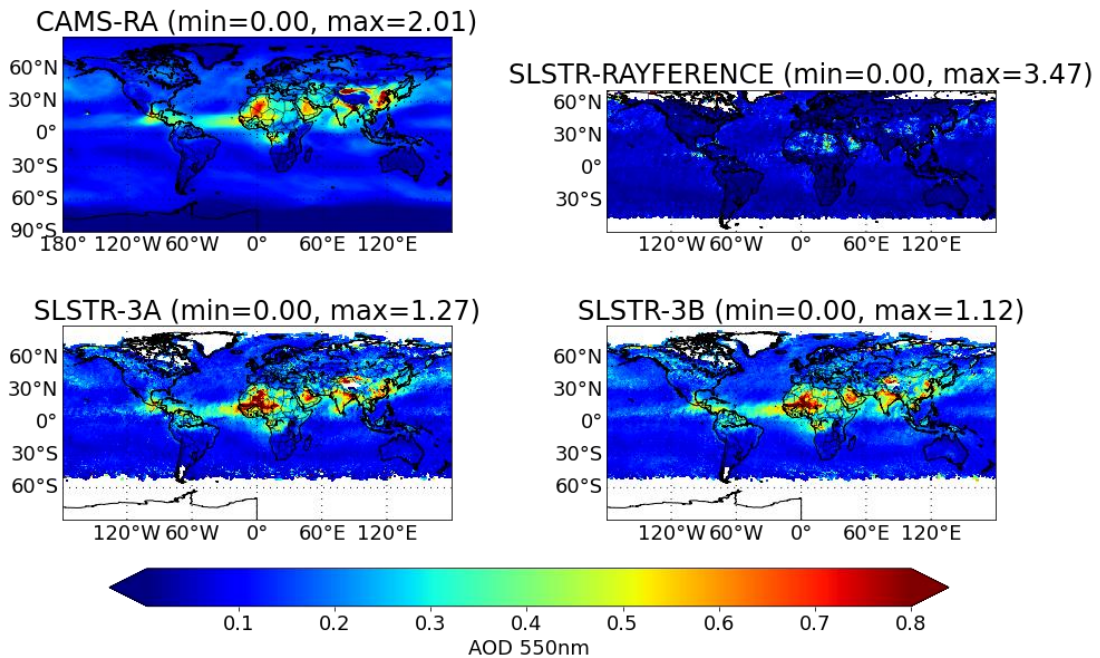


Figure 4.16 Same as figure 4.13 but for April 2020.

(a)

mean AOD 550 nm (May 2020)



(b)

mean AOD 550 nm diff w.r.t. CAMS-RA (May 2020)

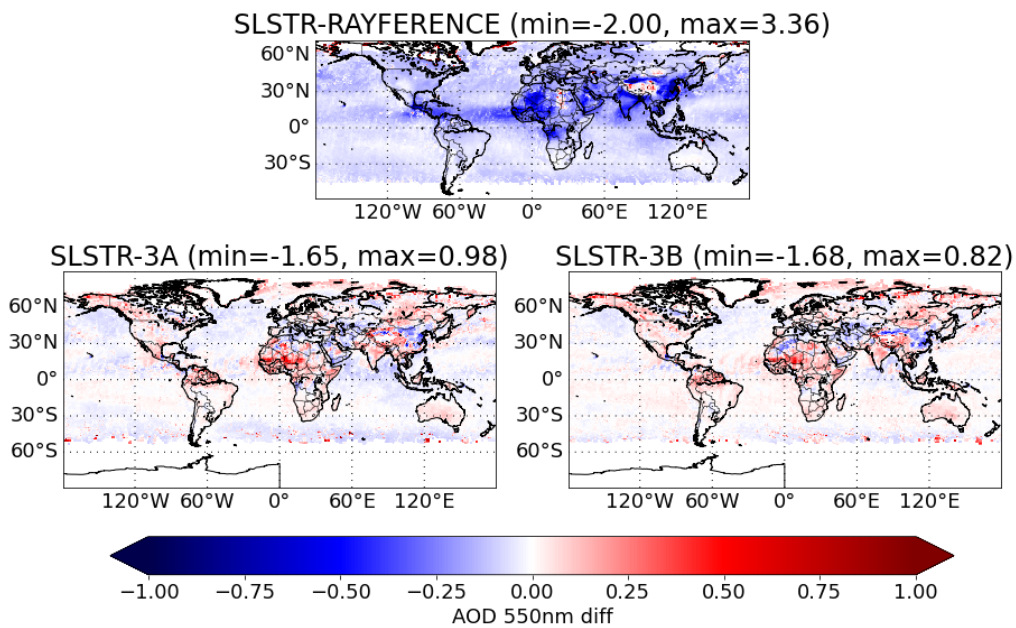
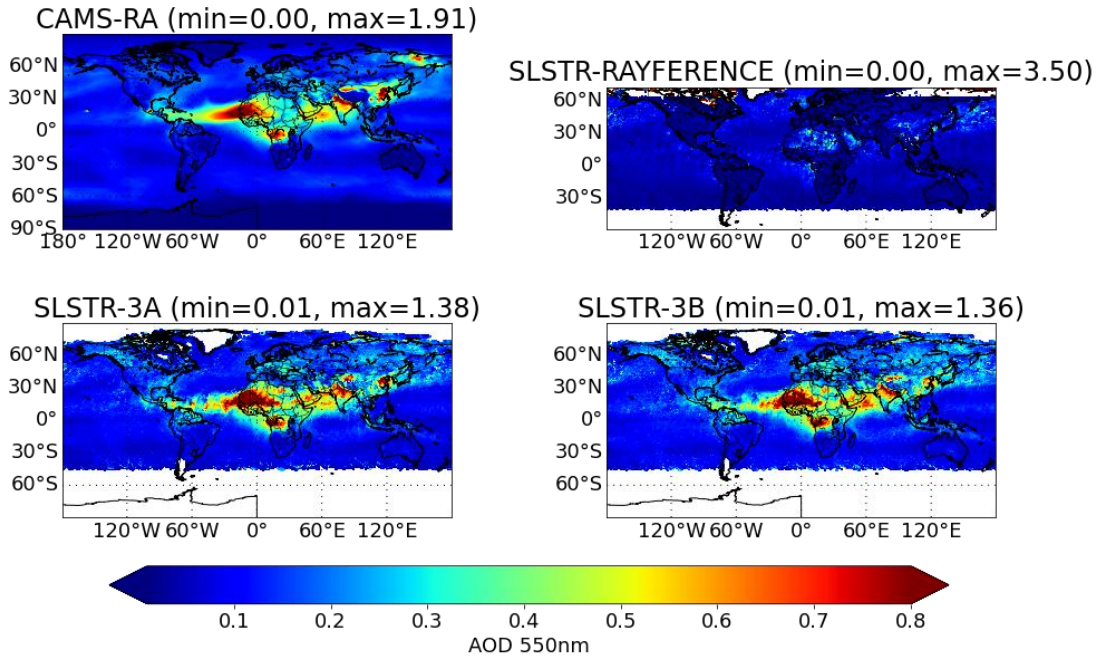


Figure 4.17 Same as figure 4.13 but for May 2020.

(a)

mean AOD 550 nm (June 2020)



(b)

mean AOD 550 nm diff w.r.t. CAMS-RA (June 2020)

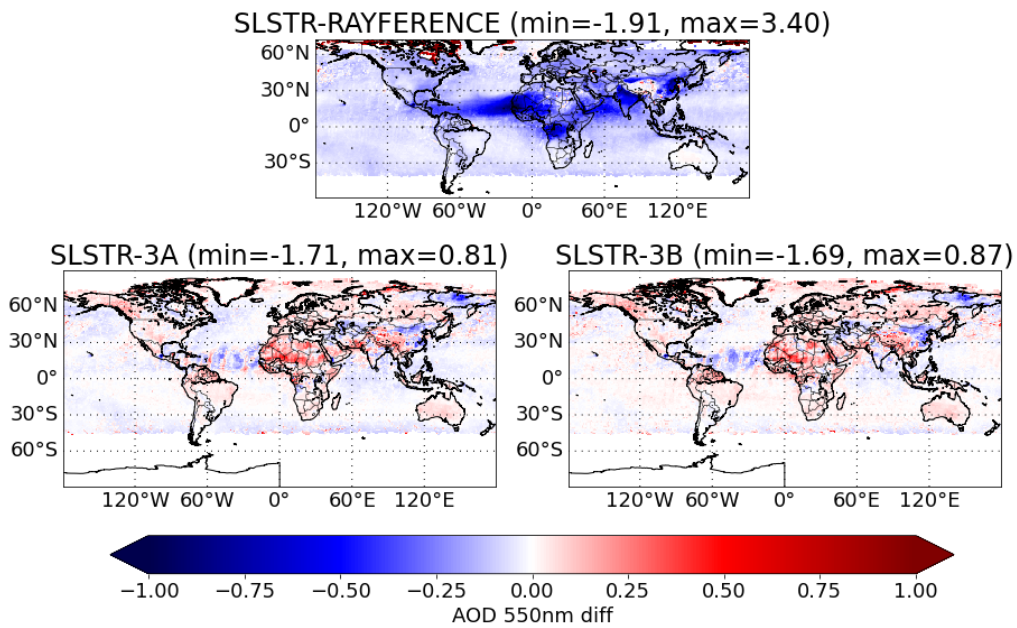
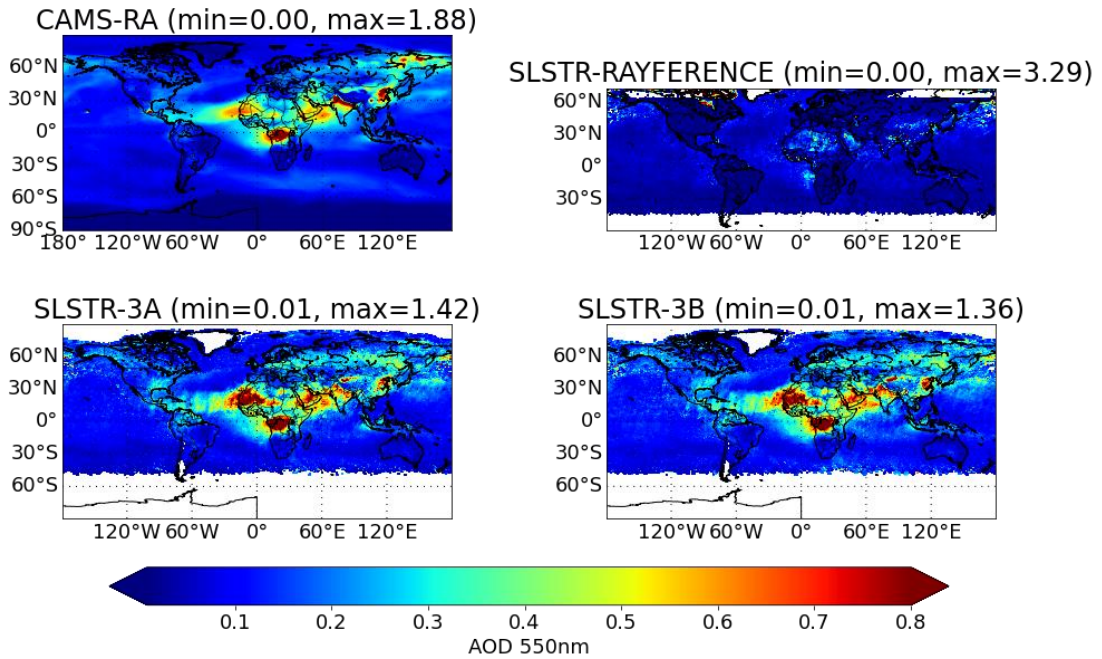


Figure 4.18 Same as figure 4.13 but for June 2020.

(a)

mean AOD 550 nm (July 2020)



(b)

mean AOD 550 nm diff w.r.t. CAMS-RA (July 2020)

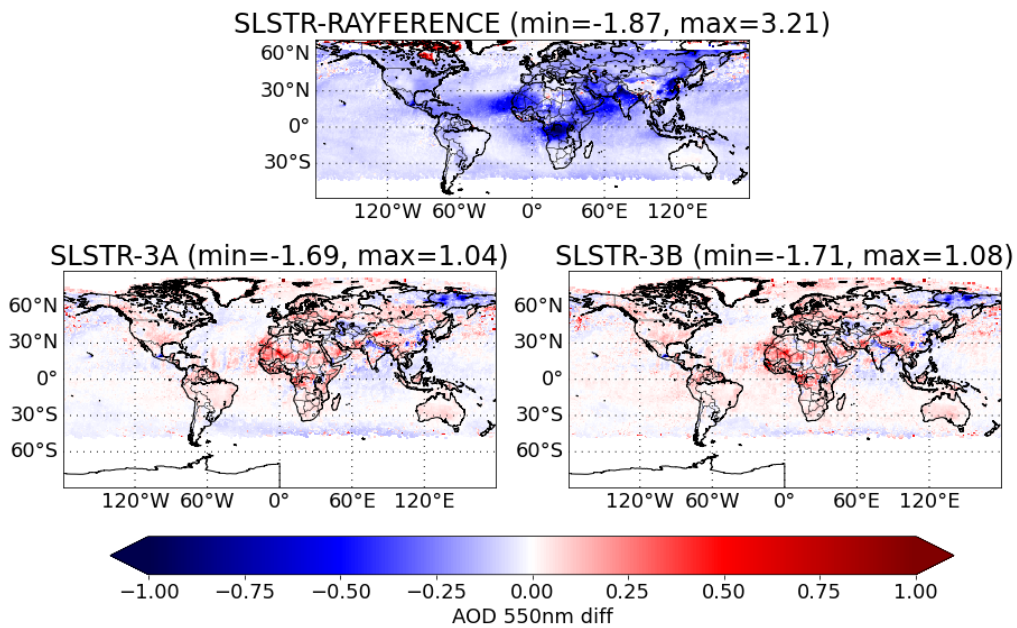
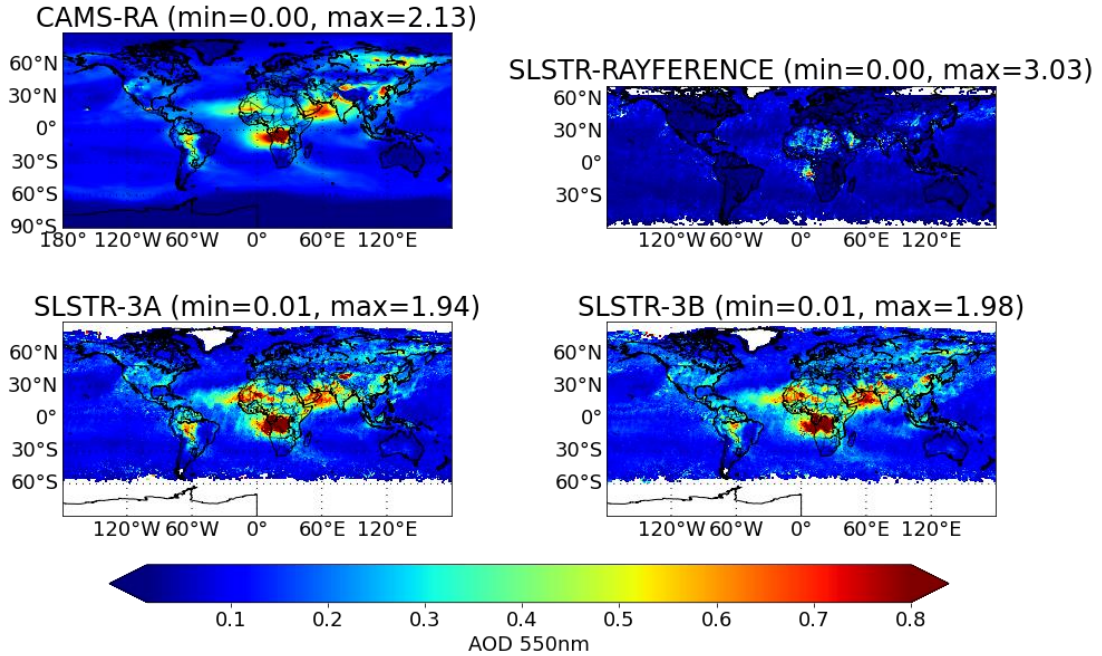


Figure 4.19 Same as figure 4.13 but for July 2020.

(a)

mean AOD 550 nm (August 2020)



(b)

mean AOD 550 nm diff w.r.t. CAMS-RA (August 2020)

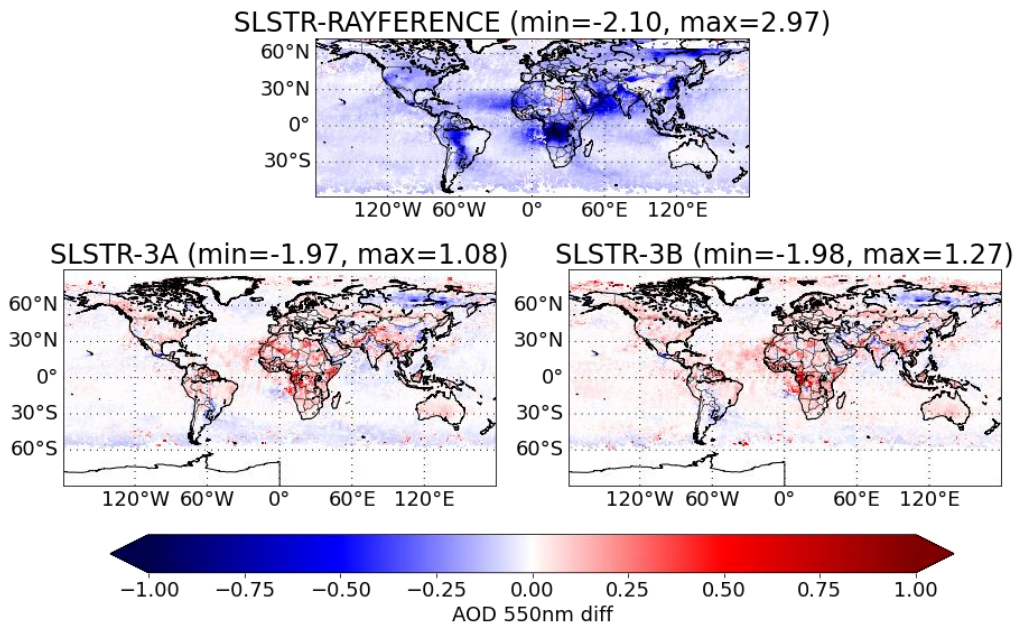
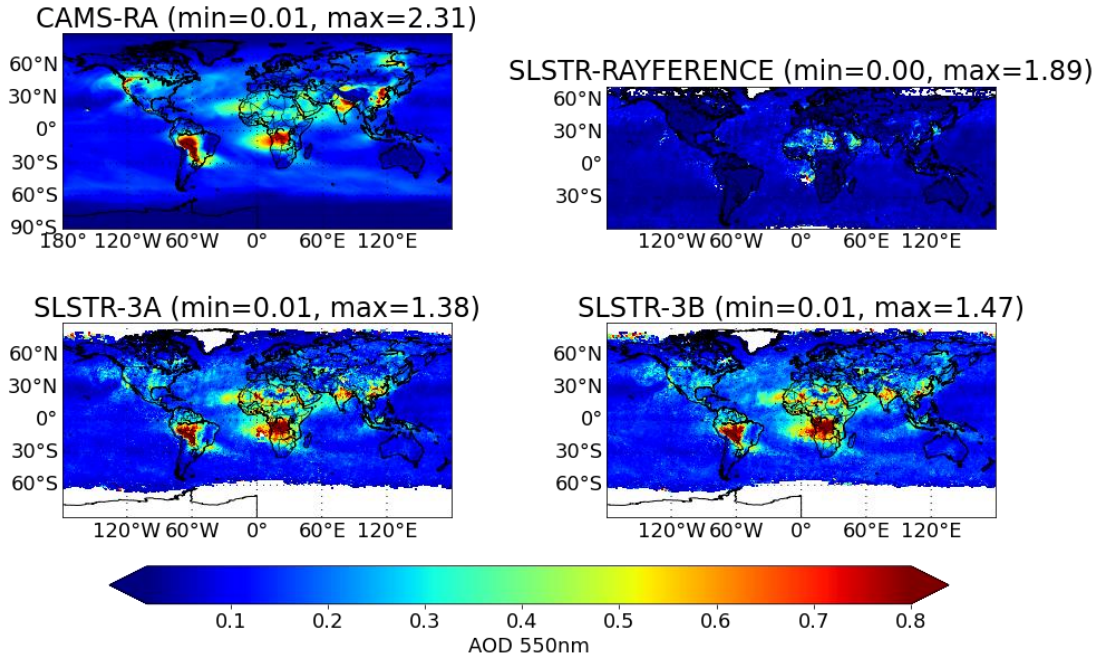


Figure 4.20. Same as figure 4.13 but for August 2020.

(a)

mean AOD 550 nm (September 2020)



(b)

mean AOD 550 nm diff w.r.t. CAMS-RA (September 2020)

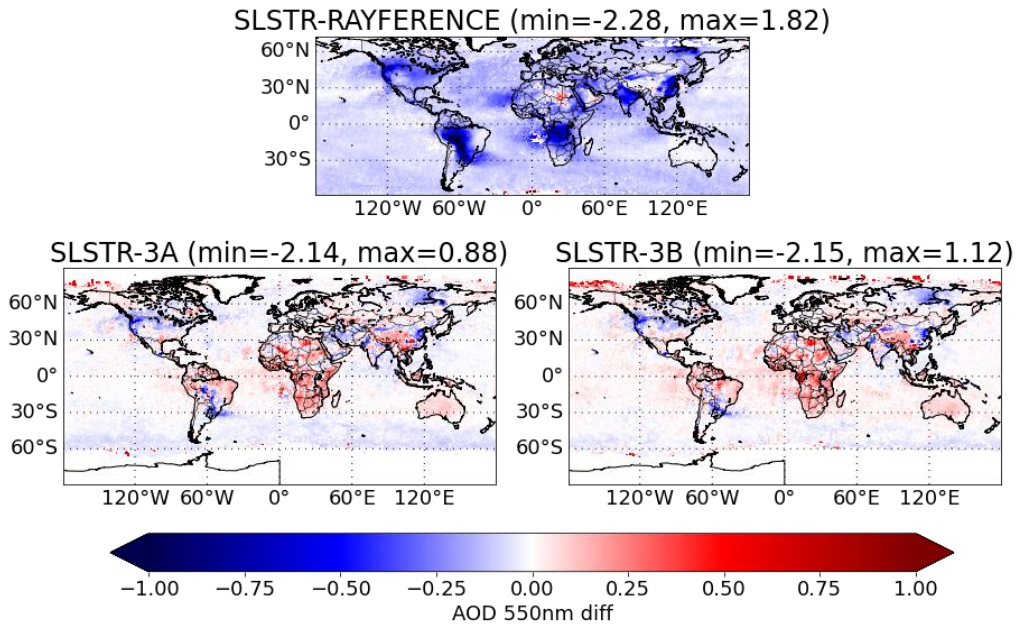
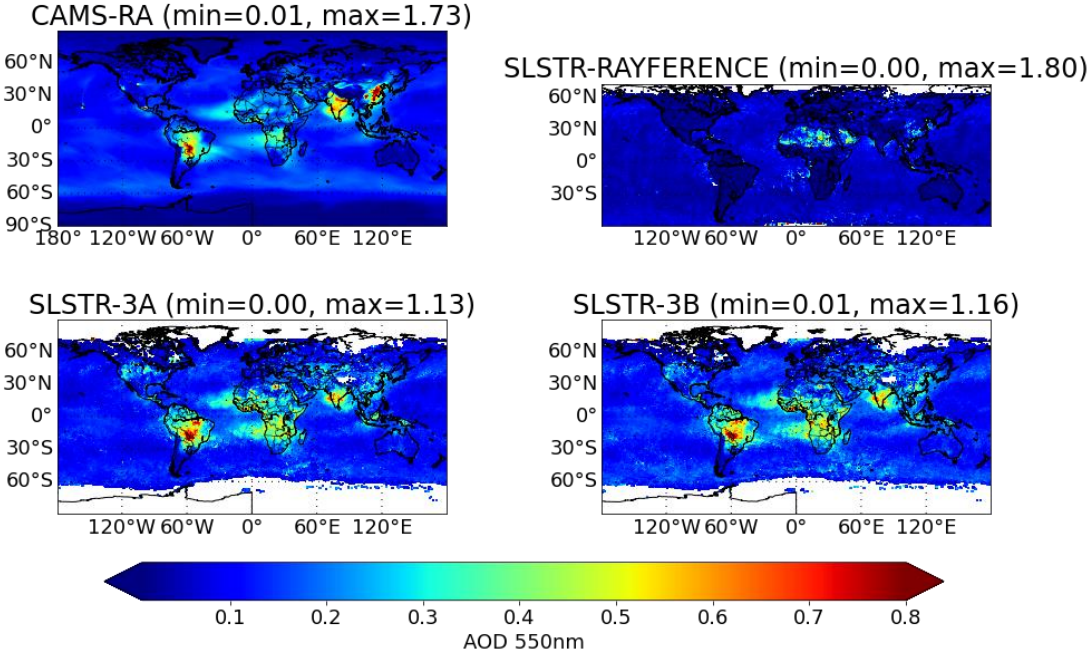


Figure 4.21 Same as figure 4.13 but for September 2020.

(a)

mean AOD 550 nm (October 2020)



(b)

mean AOD 550 nm diff w.r.t. CAMS-RA (October 2020)

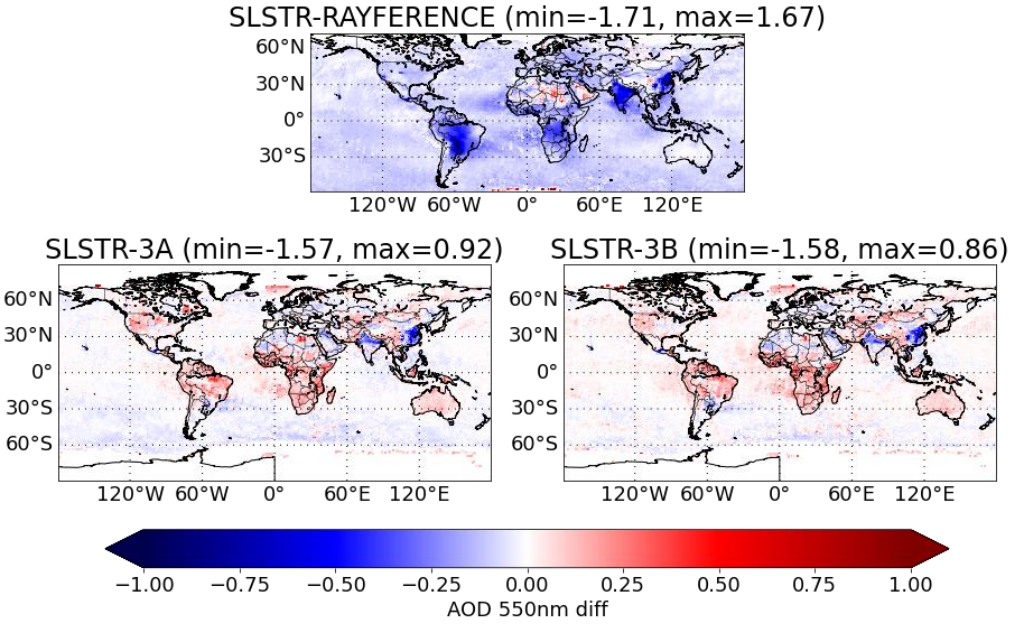
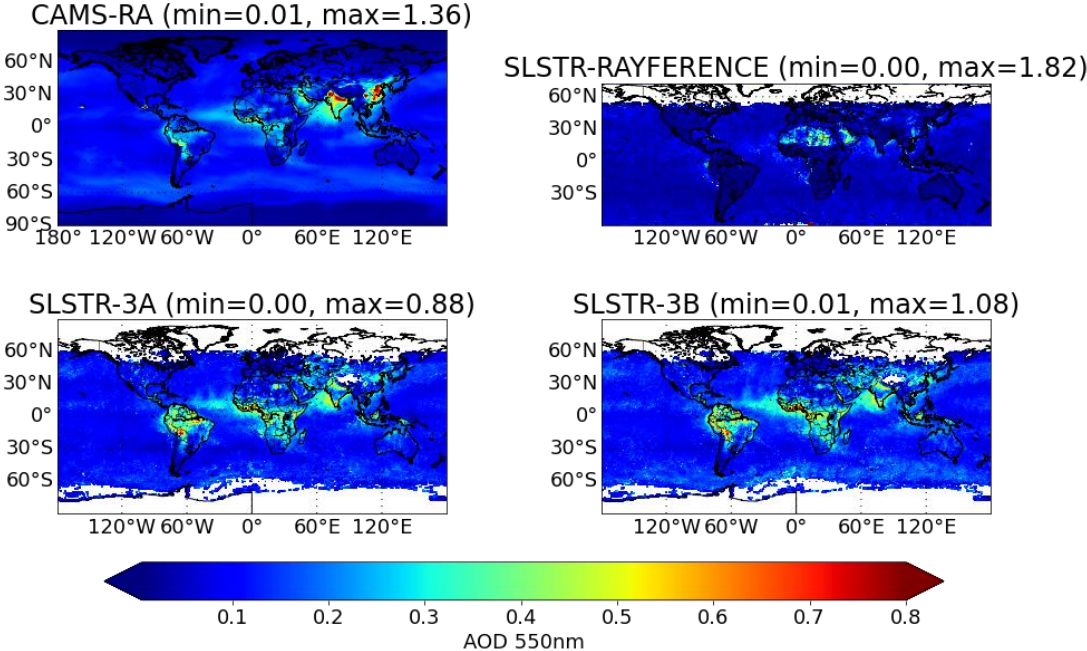


Figure 4.22 Same as figure 4.13 but for October 2020.

(a)

mean AOD 550 nm (November 2020)



(b)

mean AOD 550 nm diff w.r.t. CAMS-RA (November 2020)

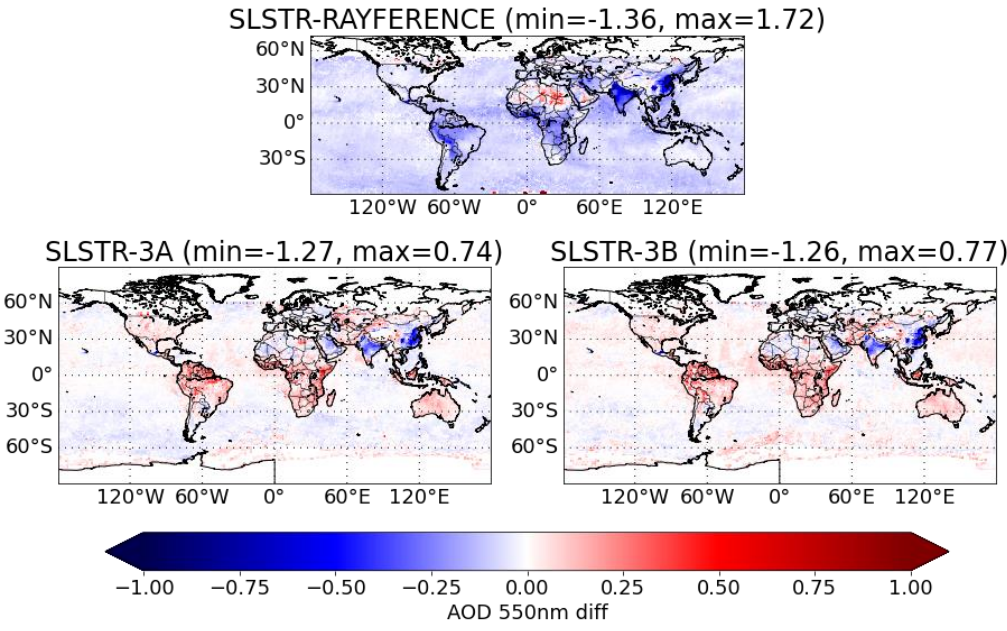
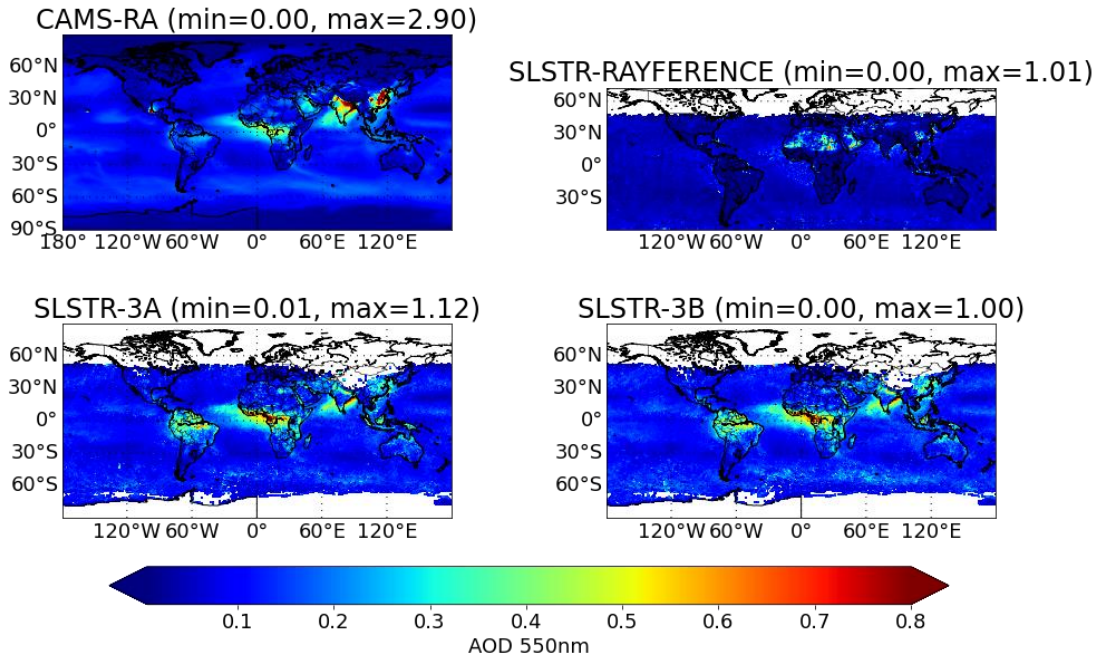


Figure 4.23 Same as figure 4.13 but for November 2020.

(a)

mean AOD 550 nm (December 2020)



(b)

mean AOD 550 nm diff w.r.t. CAMS-RA (December 2020)

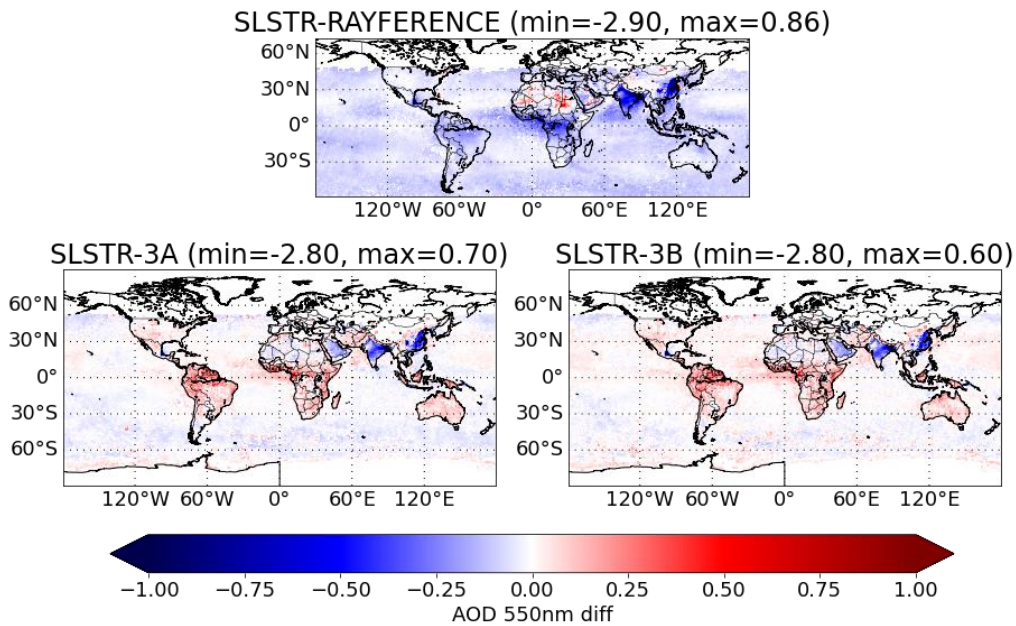


Figure 4.24 Same as figure 4.13 but for December 2020.

Data preparation of the SU SLSTR v1.14 AOD data for the assimilation experiments


The SLSTR AOD level 2 data were downloaded from ICARE and converted into BUFR format (thanks to Roberto Ribas). The format is similar to that used for AATSR data and is currently being used for the experimentation with the SLSTR NRT stream produced by EUMETSAT.

Assimilation experiments

The assimilation experiments with ECMWF's IFS in the CAMS configuration planned in the previous section have been run for the full month of September 2019 on ECMWF's supercomputer. With respect to the initial plan additional experiments were included. This was due to coordination with Sebastien Garrigues (CAMS) who is using the SLSTR NRT product from EUMETSAT (over ocean only). The table below summarizes all experiments.

Table 4.1: Overview of assimilation experiments

Experiment ID	SLSTR data	Additional Datasets (PMAP and MODIS)	Thinning (SLSTR)	Bias correction (SLSTR)	Notes
h7c4	-	-	-	-	Control (CAMS forecast only, different cycle)
hju4	no	no	no	no	Control (analysis)
hjzt	no	yes	-	-	Operational CAMS configuration
hjf2	over ocean only	yes	no	no	Same configuration as SG's experiments
hjlb	over ocean only	no	no	no	Impact of SLSTR data only over ocean
hjlc	over land and ocean	yes	no	no	Impact of SLSTR data over ocean and land
hjld	over land and ocean	no	no	no	Impact of SLSTR data only over ocean
hjxo	over ocean only	yes	yes	yes	Impact of thinning and varBC of SLTR data
hjxp	over ocean only	no	yes	yes	Impact of thinned and bias-corrected SLSTR only data over ocean
hjsxq	over land and ocean	yes	yes	yes	Impact of thinning and varBC of SLTR data
hjsxr	over land and ocean	no	yes	yes	Impact of thinned and bias-corrected SLSTR only data over land and ocean

	Aerosol_cci+ Climate Assessment Report	REF : aerosol CAR ISSUE : 3.1 DATE : 19.07.2022 PAGE : 48
---	---	--

The impact of the various datasets was assessed using the standard AERONET verification which is applied operationally in CAMS. In the standard operational CAMS configuration MODIS data are used as anchor (without any bias correction), whereas PMAP data are bias-corrected. Both PMAP and MODIS data are thinned to a resolution of 0.5x0.5 degrees. For this reason, it was decided to experiment with and without thinning for the SLSTR. Results from the evaluation using AERONET L2.0 AOD retrievals are shown below.

Verification using AERONET observations

This verification is based on ver0D which is the verification packaged for surface parameters developed by Luke Jones at ECMWF for CAMS routine monitoring (see appendix A). The plots that follow are relative to experiments hju4 (control), hjld (SLSTR AOD only in addition to CAMS standard configuration using MODIS as anchor and PMAP with bias correction based on MODIS), hjlc (SLSTR and MODIS and PMAP AOD) and hizt (CAMS standard configuration using MODIS and PMAP AOD with MODIS as anchor). The first thing to observe in all statistics shown is that there is a marked difference between the control and the assimilation experiments, namely the bias for the control is negative whereas the assimilation introduces a positive bias. This is particularly evident in the plots as a function of forecast range, when at the beginning of the integration there is a “kick” in model AOD coming from the inclusion of AOD observations, but this is not sustained in the rest of the forecast, and at the end of the integration window (5 days for the standard CAMS configuration), there is a “loss” of mass with the model AOD tending to return to the forecast only values (figure 4.30). The other striking feature is that there is very little difference between assimilating the SLSTR only and the SLSTR in addition to PMAP and MODIS. We believe that this is due to the fact that in these experiments no thinning is applied to SLSTR which dominates the signal, having approximately a factor 10 of data more than PMAP and MODIS being assimilated. Moreover, the SLSTR data are not bias-corrected. To understand the impact of applying (or not) the thinning and the bias correction, additional experiments have been run (see Table 4.1). No clear signal of the impact of thinning and bias-correcting the SLSTR data is visible in those experiments, possibly due to a problem with the set-up using MODIS as anchor. These need to be analyzed again and possibly re-run.



FC-OBS bias. Model against L2.0 Aeronet AOT at 500nm.
261 Voronoi-weighted sites globally ($r_{max}=1276\text{km}$).
1-30 Sep 2019. FC start hrs=00Z. T+6 to 24.

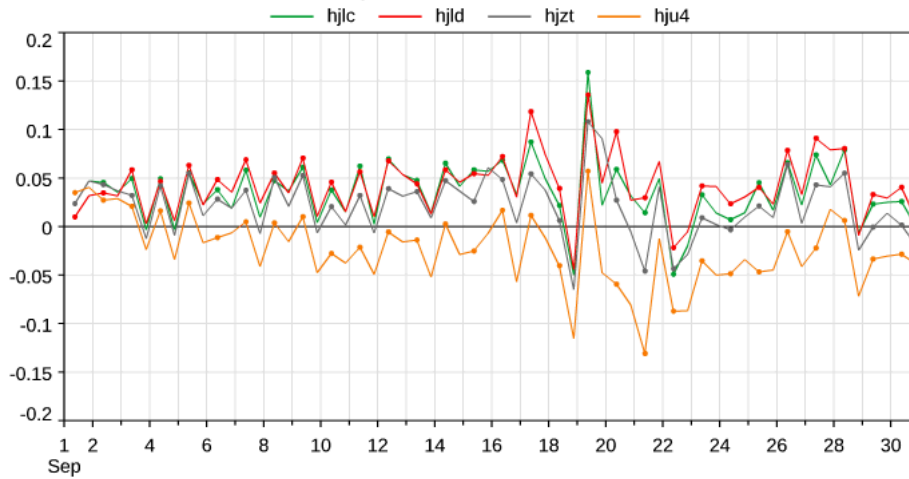


Figure 4.25. Time series of AERONET AOD FC-Obs bias at 500nm for control experiment with no AER data (yellow line), SLSTR AOD only (red line), SLSTR plus MODIS and PMAP AOD (green line) and MODIS and PMAM AOD (grey line).

RMS error. Model against L2.0 Aeronet AOT at 500nm.
261 Voronoi-weighted sites globally ($r_{max}=1276\text{km}$).
1-30 Sep 2019. FC start hrs=00Z. T+6 to 24.

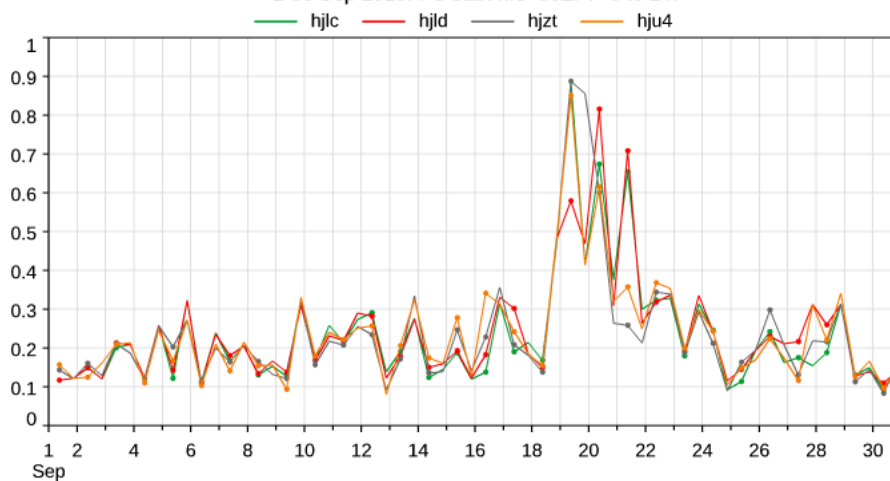


Figure 4.26. Same as figure 4.13 but for Root Mean Square (RMS) error.



Mod Norm Mean Bias. Model against L2.0 Aeronet AOT at 500nm.
261 Voronoi-weighted sites globally ($r_{max}=1276km$).
1-30 Sep 2019. FC start hrs=00Z. T+6 to 24.

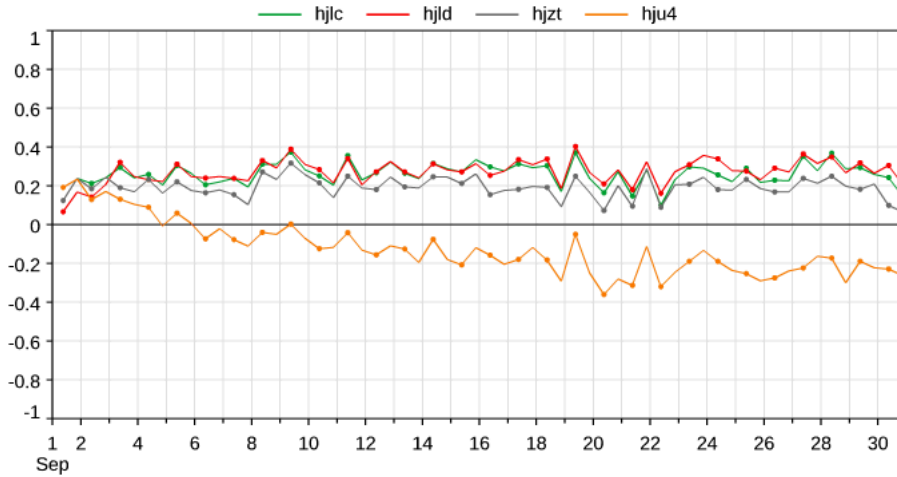


Figure 4.27. Same as figure 4.13 but for Modified Normalized Mean Bias (MNMB).

Fractional Gross Error. Model against L2.0 Aeronet AOT at 500nm.
261 Voronoi-weighted sites globally ($r_{max}=1276km$).
1-30 Sep 2019. FC start hrs=00Z. T+6 to 24.

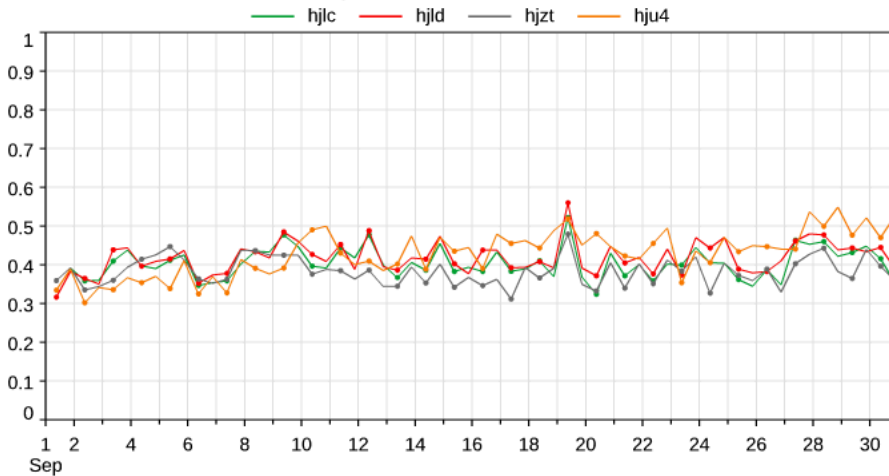


Figure 4.28. Same as figure 4.13 but for Fractional Gross Error (FGE).

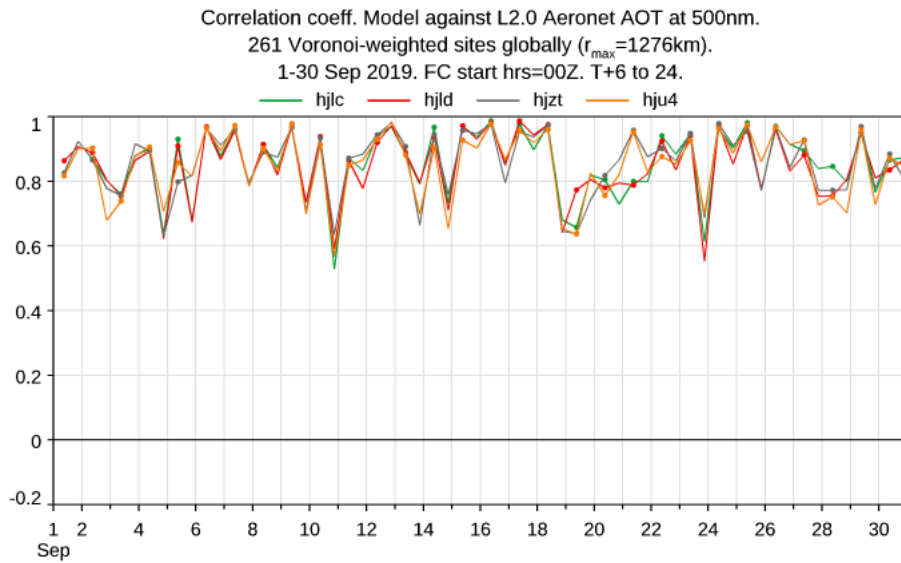


Figure 4.29. Same as figure 4.13 but for Correlation coefficient.

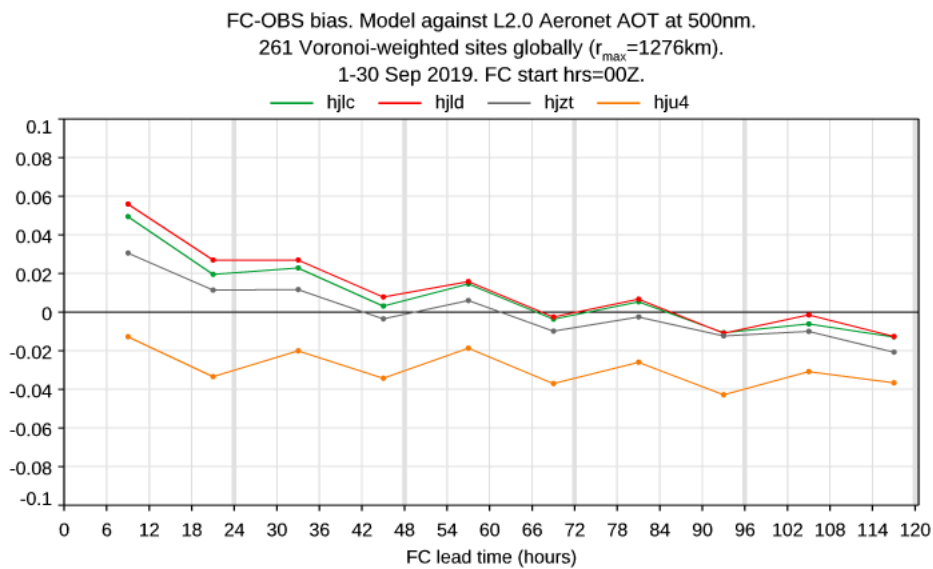


Figure 4.30. Same as figure 4.13 but as a function of forecast range.



RMS error. Model against L2.0 Aeronet AOT at 500nm.
261 Voronoi-weighted sites globally ($r_{max}=1276\text{km}$).
1-30 Sep 2019. FC start hrs=00Z.

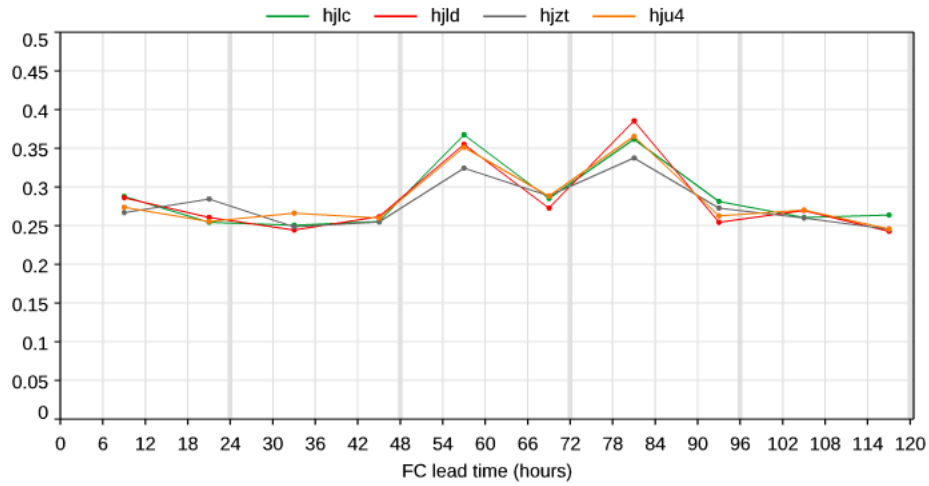


Figure 4.31. Same as figure 4.18 but for RMS error.

Mod Norm Mean Bias. Model against L2.0 Aeronet AOT at 500nm.
261 Voronoi-weighted sites globally ($r_{max}=1276\text{km}$).
1-30 Sep 2019. FC start hrs=00Z.

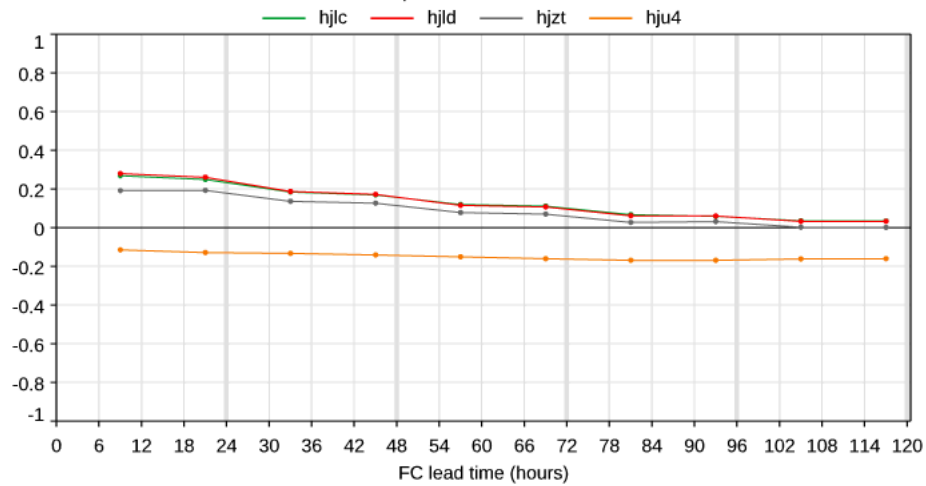


Figure 4.32. Same as figure 4.18 but for MNMB error.

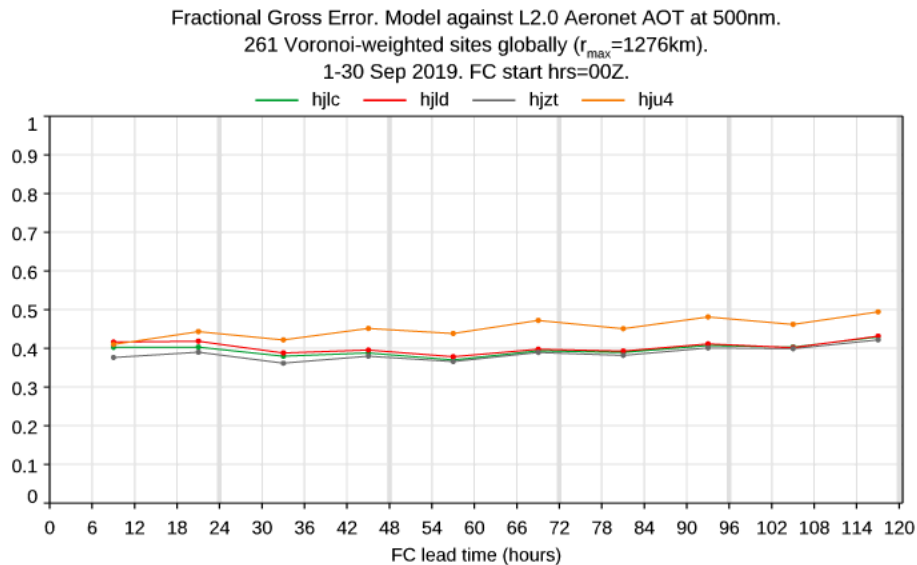


Figure 4.33. Same as figure 4.18 but for Fractional Gross error.

5 SUMMARY

Quick overview analysis of the Aerosol_cci+ test datasets were made in comparison to model (CAM5 reanalysis and MAC climatology) and other satellite datasets (MISR, MODIS).

Radiative forcing

A user case study was applied to ATSR-2 1998, AATSR 2008 and SLSTR 2020 AOD and AODf retrievals to determine aerosol associated radiative effects and climate forcing by applying data yield similar impact. The climate cooling by today's anthropogenic aerosol is near -0.9 W/m^2 for all four satellite datasets, with -0.3 W/m^2 attributed to the direct (extra aerosol presence) effect and -0.6 W/m^2 attributed to the (first) indirect effect. The solar radiation at the surface is reduced by -3.0 W/m^2 , so that 2.1 W/m^2 remains for solar heating of anthropogenic aerosol layers in the atmosphere. The similar anthropogenic aerosol impacts with data from 1998, 2008 and 2020 reflect that global totals for anthropogenic aerosol did not change much over the last 20 years, despite some regional increases (e.g. India) and decreases (e.g. Europe). In comparison to anthropogenic aerosol, for the total aerosol the direct radiative (presence) effect global averages are near -1.1 W/m^2 at TOA and -6.5 W/m^2 at the surface. Both averages are less negative due to positive infrared contributions by elevated mineral dust. Many global maps were presented to demonstrate the strong regional and seasonal variability that are associated with these averages.

Data assimilation

Several data assimilation experiments with and without using SLSTR data for the full month of September 2019 (with significant biomass burning episodes) have been conducted and compared to AERONET reference to quantify the impact of assimilating the SU v1.14 SLSTR AOD for September 2019. Overall, the inclusion of this dataset does not substantially improve the performance of the standard CAM5 system which

	<p style="text-align: center;">Aerosol_cci+ Climate Assessment Report</p>	<p>REF : aerosol CAR ISSUE : 3.1 DATE : 19.07.2022 PAGE : 54</p>
---	---	--

assimilates MODIS and PMAP AOD. When SLSTR AOD is assimilated without thinning and bias correction, a clear positive bias is seen in the resulting AOD. While the experiment without any assimilated data shows a negative bias with respect to the experiment with satellite AOD included in the analysis, most of the impact comes from the assimilation of MODIS AOD which is used as anchor datasets. To come to a more robust conclusion regarding the suitability of the SLSTR SU v.14 product for the assimilation a longer period would need to be run. However, a new version of the algorithm should be tested instead. It is likely that the next CAMS reanalysis which will start in 2024 will utilize the EUMETSAT SLSTR AOD product which is based on the original SU retrieval algorithm but has been extensively modified. Also a future SLSTR version to be developed and tested under Aerosol_cci+ Phase 2 should be considered for this assimilation study.

	Aerosol_cci+ Climate Assessment Report	REF : aerosol CAR ISSUE : 3.1 DATE : 19.07.2022 PAGE : 55
---	---	--

6 REFERENCES

Antje Inness, Melanie Ades, Anna Agusti-Panareda, Jérôme Barré, Anna Benedictow, et al.,. The CAMS reanalysis of atmospheric composition. *Atmospheric Chemistry and Physics*, European Geosciences Union, 2019, 19 (6), pp.3515-3556. ([10.5194/acp-19-3515-2019](https://doi.org/10.5194/acp-19-3515-2019)). ([hal-02090480](https://hal.archives-ouvertes.fr/hal-02090480))

Aerosol_cci2 Climate Assessment Report (CAR), v2.7, 08.01.2018

Aerosol_cci2 Product Validation and Inter-comparison Report (PVIR), v3.41, 21.12.2017

Aerosol_cci2 bridging option Product Validation and Inter-comparison Report (PVIR), v4.2, 09.01.2019

Aerosol_cci+ Product Validation and Inter-comparison Report (PVIR), v3.0, 06.05.2022

Aerosol radiative effects with MACv3 and satellites retrievals

Stefan Kinne, Paul Ginoux, Peter North, Kevin Pearson, Rob Levy, Ralph Kahn, Thomas Popp, Aerosol radiative effects with MACv3 and satellites retrievals, submitted to *Atmospheric Physics and Chemistry*, 2022, in review (major revision to be submitted mid-May 2022) – the original discussion paper was published as Kinne, S., North, P., Pearson, K., and Popp, T.: Aerosol radiative effects with dual view AOD retrievals, *Atmos. Chem. Phys. Discuss.* [preprint], <https://doi.org/10.5194/acp-2021-954>, in review, 2021.

Angela Benedetti, Gianpaolo Balsamo, Souhail Boussetta, Francesca Di Giuseppe, Antje Inness, Kenta Ochi, Patricia de Rosnay, Hao Zuo, Use of ESA Climate Change Initiative data in ECMWF's Earth system model, ECMWF science blog at <https://www.ecmwf.int/en/newsletter/171/news/use-esa-climate-change-initiative-data-ecmwfs-earth-system-model>

	Aerosol_cci+ Climate Assessment Report	REF : aerosol CAR ISSUE : 3.1 DATE : 19.07.2022 PAGE : 56
---	---	--

APPENDIX A

Ver0D is a verification tool developed by Luke Jones (CAMS) that can compare model data with point-like (i.e. zero-dimensional, hence the "0D") observations in fixed locations. The observations may be in-situ measurements (e.g. surface trace gas concentrations) or vertical-integral measurements (e.g. total-columns). It can verify multiple experiments and parameters side-by-side in the same plots. It can produce a set of plots of model vs observations for individual sites, verification statistics as a function of time, location and forecast range. It can also provide Taylor diagrams and model vs observation scatter/intensity plots.

The system is non-interactive; when it is run it generates all requested plots in a single session and writes them to disk. The plots can then later be browsed in a web page. It consists of a control layer written in Python and a compute/plot layer written in IDL and can run on the desktop workstations or the Linux cluster.

Schematically, the system is run as follows. The user decides which experiments they would like to verify side-by-side; creates a retrieval settings file for each experiment (if not already created) detailing which parameters, steps, forecast hours should be retrieved; runs jobs to retrieve and process the model data, which will be interpolated to all known observation locations and stored in a directory owned by them; creates a verification settings file governing all aspects of the verification, i.e. which observation sources to use, what plots to make, which model and observations parameters should be paired, etc.; runs the verification task of Ver0D to produce the plots; and finally browses the plots in a web page.

The following metrics are available from the ver0D package:

- The mean bias error (also known as bias, BE) captures the average deviations between two datasets (i.e. model, c , and observations, o). It has the units of the variable. Values near 0 are the optimal, negative values indicate underestimation and positive values indicate overestimation.

$$BE = \frac{1}{n} \sum_{i=1}^n (c_i - o_i)$$

- The root mean square error (RMSE) combines the spread of individual errors. It is strongly dominated by the large values, due to the squaring operation. Especially in cases where prominent outliers occur, the usefulness of RMSE is questionable and the interpretation becomes difficult.

$$RMSE = \sqrt{\frac{1}{n} \sum_{i=1}^n (c_i - o_i)^2}$$

- The correlation coefficient (r) indicates the extent to which patterns in the model match those in the observations.



$$r = \frac{\sum_{i=1}^n (c_i - \bar{c}) \cdot (o_i - \bar{o})}{\sqrt{\sum_{i=1}^n (c_i - \bar{c})^2} \cdot \sqrt{\sum_{i=1}^n (o_i - \bar{o})^2}}$$

- The fractional gross error (FGE) is a measure of model error, ranging between 0 and 2 and behaves symmetrically with respect to under- and overestimation, without over emphasizing outliers.

$$FGE = \frac{2}{n} \sum_{i=1}^n \frac{|c_i - o_i|}{|c_i + o_i|}$$

- The Modified (Normalized) Mean Bias (MMB, also called MNMB) is normalized by the mean of the observed and modelled values. This modified mean bias ranges between -2 and 2. The closer to 0 the value, the better the forecast (f).

$$B'_n = \frac{2}{N} \sum_i \left(\frac{f_i - o_i}{f_i + o_i} \right)$$

The calculation of scores is complicated by the geographic inhomogeneity of the observation sites. AERONET sites are not spread evenly over the globe but are far more concentrated in Europe and the USA. The sites in use are also time-varying, with new sites appearing and old sites disappearing. Taking simple means over the sites therefore leads to scores which reflect the geographic spread of the sites at the time and which are strongly biased towards certain regions. The observation value at a model validity time is the centred integral mean of all the observations within the time window specified by the "pre-meaning period" setting. If this is zero it's the number of observations are considered missing for that time. In this evaluation, we used 12 h window for AOD and Angstrom Exponent, and 24 h window for PM2.5 and PM10.

In order to reduce geographic bias and increase long-term stability, model-versus-AERONET scores are computed using weights for each observation that reflect the local observation density at the observation time. This is done through the calculation of "Voronoi polygons". These are the polygons defined around the AERONET stations. For a given set of points in space, the Voronoi polygon around a given point is the region closer to that point than any other. At each observation time, the polygons are calculated on the sphere for all available sites, and the polygon areas are used as the observation weights. Since the polygons will naturally be smaller in data-dense areas, observations in these areas receive lower weights than those in data-sparse areas. To prevent observations in very data-sparse areas receiving higher than reasonable weights, the polygon edges are limited to a maximum radius. This is currently set to a value which results in a maximum polygon area of 1% of the total area being scored. The model value is calculated at the station location by bilinear interpolation, independently of the polygon. The polygon just determines the weight. It is not straightforward to determine to which spatial distance does the 1% correspond typically in our case because of the big range of cases. For stations far from others, the spatial distance is the max radius stated in the plot title. In regions which are densely populated with stations it's typically much lower, hence giving an average wouldn't be very meaningful. Please refer to the global AERONET map in figure AA.1 for an idea of the average distance between stations.

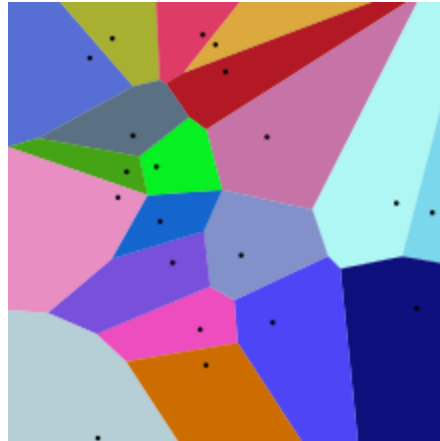


Fig. AA.1 Example of Voronoi polygons.

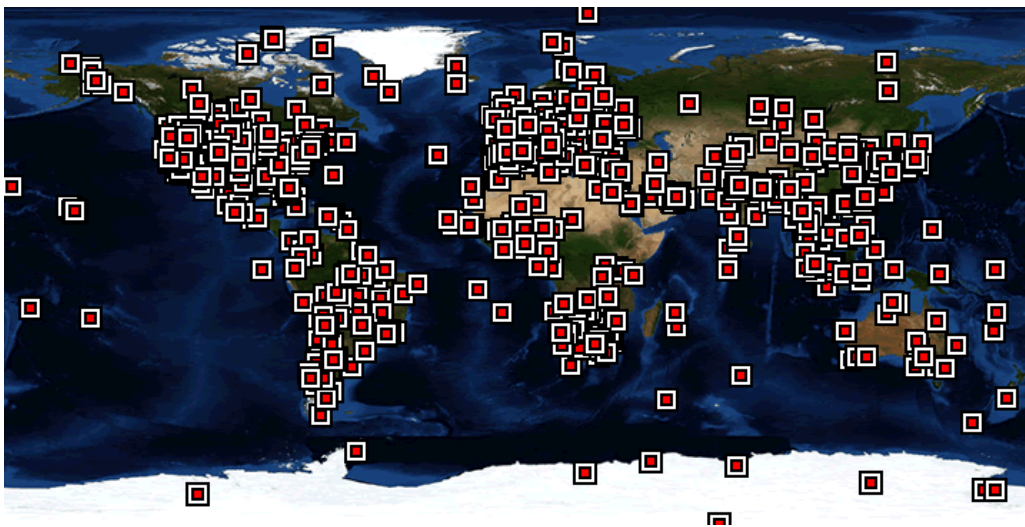


Fig. AA.2 AERONET station map (source: <https://aeronet.gsfc.nasa.gov>).



Aerosol_cci+
Climate Assessment Report

REF : aerosol CAR
ISSUE : 3.1
DATE : 19.07.2022
PAGE : 59

End of the document